

Probing Large Extra Dimension at DUNE using beam tunes

Kim Siyeon^{1,2} ^a, Suhyeon Kim^{1,2} ^b, Mehedi Masud¹ ^c, Juseong Park^{1,2} ^d

¹ *High Energy Physics Center, Chung-Ang University, Seoul 06974, Korea*

² *Department of Physics, Chung-Ang University, Seoul 06974, Korea*

Abstract

The Deep Underground Neutrino Experiment (DUNE) is a leading experiment in neutrino physics which is presently under construction. DUNE aims to measure the yet unknown parameters in the three flavor oscillation case which includes discovery of leptonic CP violation, determination of the neutrino mass hierarchy and measuring the octant of θ_{23} . Additionally, the ancillary goals of DUNE include probing the subdominant effects induced by possible physics beyond the Standard Model (BSM). One such new physics scenario is the possible presence of Large Extra Dimension (LED) which can naturally give rise to tiny neutrino masses. LED impacts neutrino oscillation through two new parameters, - namely the lightest Dirac mass m_0 and the radius of the extra dimension R_{ED} ($< 2 \mu\text{m}$). At the DUNE baseline of 1300 km, the probability seems to be modified more at the higher energy ($\gtrsim 4-5 \text{ GeV}$) in presence of LED. In this work, we attempt to constrain the parameter space of m_0 and R_{ED} by performing a statistical analysis of neutrino data simulated at DUNE far detector (FD). We illustrate how a combination of the standard low energy (LE) neutrino beam and a medium energy (ME) neutrino beam can take advantage of the relatively large impact of LED at higher energy and improve the constraints. In the analysis we also show the role of the individual oscillation channels ($\nu_\mu \rightarrow \nu_e, \nu_\mu \rightarrow \nu_\mu, \nu_\mu \rightarrow \nu_\tau$), as well as the two neutrino mass hierarchies.

^aEmail: siyeon@cau.ac.kr

^bEmail: sua8897@gmail.com

^cEmail: masud@cau.ac.kr

^dEmail: juseongpark0921@gmail.com

1 Introduction

The phenomenon of neutrino oscillation has been firmly established from the analysis of atmospheric [1] and solar [2] neutrino experiments, which provide an irrefutable evidence that neutrinos are massive particles. Various other experiments have confirmed neutrino oscillation till date. The global analyses of oscillation data [3–7] are mostly consistent with the standard three-flavor (ν_e, ν_μ, ν_τ) neutrino scenario, fully described by three mixing angles $\theta_{12}, \theta_{13}, \theta_{23}$; one CP phase (δ_{13}) and two mass squared differences Δm_{31}^2 , and Δm_{21}^2 . However, there still remains several unanswered questions in the neutrino sector. One such crucial issue is how neutrino gains its tiny mass, since in the Standard Model (SM), neutrinos are massless particles. In order to explain the small neutrino masses, in the traditional approach, the SM is extended to include heavy right handed (RH) neutrinos to generate the tiny masses of the neutrinos via *seesaw* mechanism [8–11].

But there is also an alternative mechanism to generate the small neutrino masses in presence of a new physics model known as Large Extra Dimension (LED). The model of LED was originally developed to address another fundamental problem, - the huge gap between the electroweak scale ($M_{EW} \sim 10^3$ GeV) and the Planck scale ($M_{pl} \sim G_N^{-1/2} \sim 10^{18}$ GeV) (also known as the *hierarchy problem*) [12–14]. In this model, the familiar 4-dimensional spacetime forms a hypersurface (known as *brane*) embedded within a higher dimensional ($4 + n$ dimension) spacetime, known as the *bulk*, - n being the number of extra spatial dimensions with size R . The SM particles (quarks, leptons and gauge bosons) reside in the brane, while gravity can propagate in the bulk (full $4 + n$ dimensions), - making gravity orders of magnitude weaker in strength compared to other fundamental interactions. If R is the radius of the extra dimension, then at a distance $r \lesssim R$, the gravitational force falls off as $r^{-(2+n)}$, while at $r > R$, it retains its usual r^{-2} falloff. In LED, the electroweak scale is the only fundamental mass scale ($M_f \sim M_{EW} \sim \mathcal{O}(1 \text{ TeV})$) and it is related to the Planck scale as $M_{pl}^2 \simeq M_f^{2+n} R^n$. This gives the size of the extra spatial dimensions as $R \sim 2 \times 10^{(30/n)-17}$ cm. One extra spatial dimension ($n = 1$) gives $R \sim 10^8$ km, which indicates deviations of gravitational force at solar-scale distances and is thus easily excluded from astrophysical observations. But $n \gtrsim 2$ suggests deviations of gravitational force at $\mathcal{O}(10^{-1})$ mm or below. Thus two or more extra spatial dimensions are still allowed and may potentially be detected at future experiments.

LED can explain the smallness of neutrino mass in an elegant way [15–19]. Since the RH neutrinos are singlets under SM gauge group, they can propagate into the bulk. The left handed (LH) neutrinos which are $SU(2)$ doublets in SM are restricted to the brane only. Thus the Yukawa couplings between the RH neutrinos and the SM LH neutrinos are suppressed by a factor of M_{EW}^2/M_{pl} and this in turn gives the smallness of neutrino mass. The existence of LED can be probed in neutrino experiments through the effects of Kaluza-Klein (KK) excitations which describe the RH neutrinos in the bulk. The KK modes describing the higher dimensional RH neutrino fields behave like an infinite tower of sterile neutrinos. They induce additional frequencies in the oscillation probabilities and generate distortion in a subdominant way. The usual practice is to consider an asymmetric space where only one out of n extra spatial dimensions is large, such that there are four spatial dimensions in total. Two additional parameters appear in the neutrino oscillation phenomenology in presence of LED, - namely the lightest neutrino mass (m_0) and the radius/size of the extra

dimension (R_{ED}).

Several next-generation long-baseline neutrino experiments are in the pipeline in order to explore the unresolved issues in neutrino oscillation physics,- such as, the search for leptonic CP violation (CPV), determination of neutrino mass hierarchy and the correct octant of the mixing angle θ_{23} *etc.*. These future experiments include, for *e.g.*, Deep Underground Neutrino Experiment (DUNE) [20, 21], Tokai to Hyper-Kamiokande (T2HK) [22], Tokai to Hyper-Kamiokande with a second detector in Korea(T2HKK) [23], European Spallation Source ν Super Beam (ESS ν SB) [24] among others. Due to the unprecedented precisions these future neutrino facilities are expected to achieve, they are also sensitive to the effects of new physics such as the presence of LED. In the present work we focus on DUNE and explore its capability to probe the relevant LED parameter space of $(m_0 - R_{\text{ED}})$. DUNE is expected to use the standard low energy (LE) tuned flux (having a peak around 2 – 3 GeV and falling quickly at energies $E \gtrsim 4$ GeV) with a total runtime of 13 years distributed equally between the ν and $\bar{\nu}$ modes (6.5 years + 6.5 years) [25]. Among the additional fluxes that can be used at DUNE, there is a possibility of using a medium energy (ME) beam (also known as the ν_τ -optimized beam) which offers substantial statistics even at energies $E \gtrsim 4$ GeV (although at the cost of some loss of statistics around 2 – 3 GeV) [25, 26]. It has already been shown in literature that the combinations of different beams can be optimized in order to improve the sensitivity to new physics parameters and other standard unknowns [27, 28]. In this article we seek to exploit a possible optimized combination of the LE and ME beam in order to probe the LED parameters more efficiently.

In literature, there are several works that analyze the LED parameters at DUNE and other LBL experiments [29–39]. For *e.g.*, the authors of [31, 34, 35] study LED parameters at DUNE and further [31] analyzes the capability of DUNE to distinguish between different new physics scenarios such as that of LED and light sterile neutrinos. The authors of [36] have done an analysis of LED with the available data from MINOS/MINOS+ [40] and Daya Bay [41] experiments and have also projected the future constraints from direct neutrino mass measurement experiments like KATRIN [42]. The author of [38] has probed the LED parameters using both the charged-current and neutral current interactions at DUNE and also compared the results by estimating sensitivities from other LBL experiments such as T2HK and ESS ν SB. Most recently, the authors of [39] have analyzed the sensitivities to LED parameters at DUNE when using a high-energy tuned beam. There are three distinct aspects in which the present work goes beyond the other existing works on LED at LBL experiments.

- In the standard analyses of LED at DUNE, the beam used is generally the standard low energy (LE)-tuned beam. In the present work we exploit the higher energy effects of LED more efficiently and use the medium energy (ME) tuned beam (ν_τ -optimised beam) in conjunction with the LE beam in order to improve the constraints on LED parameter space. We would like to emphasize that our study estimates an optimized combination of runtimes shared between the LE and ME beam so that we utilise the statistics from both the low-energy and higher-energy bins ¹.
- We include the contributions from $\nu_\mu \rightarrow \nu_\tau$ channel (in addition to $\nu_\mu \rightarrow \nu_e$ and

¹This is in contrast to the study conducted in [39] where only one high energy beam was used to constrain LED.

$\nu_\mu \rightarrow \nu_\mu$) in our analyses and also discuss the individual roles of all three channels in constraining LED.

- We use the most recent GLoBES configurations by the DUNE collaboration [43]. This has a runtime of 13 years with 624 kt.MW.yr. exposure.

The article is organized as follows. We start with a brief overview of the relevant theoretical basics of LED in Sec. 2 in the context of neutrino oscillation, and then follow it up with a probability level discussion in Sec. 3. We then discuss about the different beam tunes and the corresponding event spectra in Sec. 4. This is followed by an outline of the statistical procedure adopted in Sec. 5, followed by our main sensitivity results in Sec. 6. Finally we conclude in Sec. 7.

2 Theoretical basics of LED

In presence of LED, the fields carrying charge under the SM gauge symmetries are confined to the familiar 4d spacetime (brane) and the fields that are singlets under SM gauge symmetries can propagate into the (4+N) dimensional spacetime (bulk). Following the usual treatment of LED models in neutrino oscillation phenomenology [29, 31, 36, 38, 44–52] we consider effectively a (4+1) dimensional spacetime, such that one extra dimension is compactified on a circle with radius R_{ED} , which is much larger than the other extra dimensions. We consider three right handed neutrino fields $\nu_{\alpha R}$ (lying in the 5d spacetime) associated with the three left-handed neutrino fields $\nu_{\alpha L}$ ($\alpha = e, \mu, \tau$) residing in the 4d spacetime. The $\nu_{\alpha R}$ can be expressed as infinite number of Kaluza-Klein modes after imposing the periodic boundary conditions due to the compactification of the fifth dimension. The relevant mass term of the lagrangian after electroweak symmetry breaking becomes [29],

$$\mathcal{L}_{\text{mass}} = \sum_{\alpha, \beta} m_{\alpha\beta}^D \left[\bar{\nu}_{\alpha L}^{(0)} \nu_{\beta R}^{(0)} + \sqrt{2} \sum_{n=1}^{\infty} \bar{\nu}_{\alpha L}^{(0)} \nu_{\beta R}^{(n)} \right] + \sum_{\alpha} \sum_{n=1}^{\infty} \frac{n}{R_{\text{ED}}} \bar{\nu}_{\alpha L}^{(n)} \nu_{\alpha R}^{(n)} + h.c., \quad (1)$$

where $\alpha, \beta = e, \mu, \tau$; $m_{\alpha\beta}^D$ is the Dirac mass matrix. $\nu_{\alpha R}^{(0)}, \nu_{\alpha R}^{(n)}, \nu_{\alpha L}^{(n)}$ are the linear combinations of the bulk fermion fields that couple to the SM neutrino fields $\nu_{\alpha L}^{(0)}$, and the index n denotes the KK mode. After diagonalizing the Dirac mass matrix m^D using U and R such that $U^\dagger m^D R = \text{diag}(m_1^D, m_2^D, m_3^D)$, the mass term becomes,

$$\mathcal{L}_{\text{mass}} = \sum_{i=1}^3 \bar{\nu}'_{iL} M_i \nu'_{iR} + h.c., \quad (2)$$

where M_i is an infinite dimensional matrix:

$$M_i = \frac{1}{R_{\text{ED}}} \begin{pmatrix} m_i^D R_{\text{ED}} & 0 & 0 & \dots & 0 \\ \sqrt{2} m_i^D R_{\text{ED}} & 1 & 0 & \dots & 0 \\ \sqrt{2} m_i^D R_{\text{ED}} & 0 & 2 & \dots & 0 \\ \dots & \dots & \dots & \dots & \dots \\ \dots & \dots & \dots & \dots & \dots \\ \sqrt{2} m_i^D R_{\text{ED}} & 0 & 0 & \dots & n \end{pmatrix}. \quad (3)$$

The new basis in Eq. 2 are given by,

$$\begin{aligned}\nu_{\alpha L}^{(0)} &= \sum_i U_{\alpha i} \nu_{iL}'^{(0)}, & \nu_{\alpha R}^{(0)} &= \sum_i R_{\alpha i} \nu_{iR}'^{(0)} \\ \nu_{\alpha L,R}^{(n)} &= \sum_i R_{\alpha i} \nu_{iL,R}'^{(n)} & \text{with } n > 0.\end{aligned}\quad (4)$$

The true mass is obtained after diagonalisation of the infinite-dimensional matrix M_i and the subsequent mixing of the three active neutrinos is given by,

$$\nu_{\alpha L} = \sum_{i=1}^3 U_{\alpha i} \sum_{n=0}^{\infty} V_i^{(n)} \nu_{iL}'^{(n)}, \quad (5)$$

where U is the standard 3×3 unitary leptonic mixing matrix. $\nu_{iL}'^{(n)}$ is a neutrino field with mass $m_i^n = \lambda_i^n / R_{\text{ED}}$ where λ_i^n are the solutions of the eigenvalue equation,

$$\lambda_i^n - \pi(m_i^D R_{\text{ED}})^2 \cot(\pi \lambda_i^n) = 0. \quad (6)$$

$m_i^D (i = 1, 2, 3)$ are the three eigenvalues of the Dirac neutrino mass matrix, which are strongly suppressed by the LED volume factor equal to (M_f/M_{pl}) [17]. The eigenvalue equation has infinite number of solutions for λ_i^n in the interval $[n, n + 1/2]$ (for $n = 0, 1, 2, \dots, \infty$). This implies,

$$\frac{n}{R_{\text{ED}}} < m_i^n < \frac{n + 1/2}{R_{\text{ED}}} \quad \text{for } n = 0, 1, 2, \dots, \infty. \quad (7)$$

The elements of the mixing matrix V in Eq. 5 are given by [16, 17, 53],

$$(V_i^n)^2 = \frac{2}{1 + \pi^2(m_i^D R_{\text{ED}})^2 + (m_i^n/m_i^D)^2}. \quad (8)$$

Assuming LED to be a perturbative effect ($\xi_i = m_i^D R_{\text{ED}} \ll 1$) on top of the standard three neutrino oscillation, it is possible to solve the eigenvalue equation analytically to obtain the following approximate expressions [44].

$$\begin{aligned}m_i^0 &\simeq m_i^D \left[1 - \frac{\pi^2}{6} \xi_i^2 + \dots \right], & V_i^0 &= 1 - \frac{\pi^2}{6} \xi_i^2 + \dots, \\ m_i^n &\simeq \frac{n}{R_{\text{ED}}} \left[1 + \frac{\xi_i^2}{n^2} + \dots \right], & V_i^n &= \sqrt{2} \frac{\xi_i}{n} \left[1 - \frac{3}{2} \frac{\xi_i^2}{n^2} + \dots \right] \quad \text{for } n > 0.\end{aligned}\quad (9)$$

The neutrino oscillation probability in presence of LED from a flavour α to a flavour β is given by,

$$P_{\nu_\alpha \rightarrow \nu_\beta}^{\text{LED}} = \left| \sum_{j=1}^3 \sum_{n=0}^{\infty} U_{\alpha j}^* U_{\beta j} (V_j^n)^2 \exp\left(-i \frac{(m_j^n)^2 L}{2E}\right) \right|^2, \quad (10)$$

where E is the neutrino energy and L is the baseline length. Expanding Eq. 10, it can be seen that $P_{\nu_\alpha \rightarrow \nu_\beta}^{\text{LED}}$ contains the interference phases,

$$\phi_{jk}^{mn} = \left[(m_j^m)^2 - (m_k^n)^2 \right] \frac{L}{2E} = \Delta(m_{jk}^{mn})^2 \frac{L}{2E} \quad (j, k = 1, 2, 3; m, n = 0, 1, 2, \dots, \infty). \quad (11)$$

Further, each of these mass-induced interference terms are also proportional to the LED mixing term $(V_j^m)^2 (V_k^n)^2$ (in addition to the mixing induced by the standard PMNS matrix U). The phase differences can be seen as originating from the following three types of interferences,

- *Interferences among standard neutrinos (i.e., 0-mode KK neutrinos):* In this case the corresponding phase and the LED mixing terms in leading orders are (using Eqs. 9),

$$\begin{aligned}\phi_{jk}^{00} &= \Delta(m_{jk}^{00})^2 \frac{L}{2E}, \\ (V_j^0)^2 (V_k^0)^2 &\simeq 1 - \frac{\pi^2}{3} (\xi_j^2 + \xi_k^2) \quad (j, k = 1, 2, 3).\end{aligned}\quad (12)$$

The expressions in Eq. 12 contribute to two kinds of terms in the probability expression of Eq. 10. The terms proportional to $\exp(-i\phi_{jk}^{00})$ can be recognized roughly as the contribution from the standard oscillation probability in the three neutrino case. On the other hand, the terms proportional to $-\frac{\pi^2}{3}(\xi_j^2 + \xi_k^2)\exp(-i\phi_{jk}^{00})$ give the correction to the probability due to the presence of LED. Note that this correction has a negative sign implying that the presence of LED tends to decrease the magnitude of oscillation probability.

- *Interferences between the standard and ($n > 0$) KK mode neutrinos:* In this case, the corresponding phase and the mixing in leading orders can be derived as,

$$\begin{aligned}\phi_{jk}^{0n} &= \Delta(m_{jk}^{0n})^2 \frac{L}{2E} \simeq -\frac{n^2}{R_{\text{ED}}^2} \frac{L}{2E}, \\ (V_j^0)^2 (V_k^n)^2 &\simeq \frac{2}{n^2} \xi_k^2 \quad (j, k = 1, 2, 3; n > 0).\end{aligned}\quad (13)$$

For a typical value of $R_{\text{ED}} = 0.5 \mu\text{m} \simeq 2.5 \text{ eV}^{-1}$, the mass-squared difference corresponding to the lowest mode ($n = 1$) KK neutrino is $\Delta(m_{jk}^{01})^2 \simeq -0.16 \text{ eV}^2$, such that $|\Delta(m_{jk}^{01})^2|$ is orders of magnitude larger than the standard mass squared differences $|\Delta m_{31}^2|$ ($\sim 10^{-3} \text{ eV}^2$) and Δm_{21}^2 ($\sim 10^{-5} \text{ eV}^2$). The mass-squared differences for higher KK modes are even higher in magnitude ($\propto n^2$). Thus for the typical values of $L \sim \mathcal{O}(10^3) \text{ km}$ and $E \lesssim \mathcal{O}(10) \text{ GeV}$, the interference terms with phases ϕ_{jk}^{0n} ($n > 0$) get largely averaged out. Further, Eq. 13 shows that the corresponding interference terms are suppressed by the small perturbative term proportional to ξ_k^2 ($k = 1, 2, 3$) as well, and this suppression gets even stronger for higher KK modes ($\propto n^{-2}$).

- *Interferences among the ($n > 0$) KK mode neutrinos:* The relevant phase and the mixing factors can be shown as (in leading orders),

$$\begin{aligned}\phi_{jk}^{mn} &\simeq \frac{1}{R_{\text{ED}}^2} \left[m^2 - n^2 + 2(\xi_j^2 - \xi_k^2) \right] \frac{L}{2E}, \\ (V_j^m)^2 (V_k^n)^2 &\simeq \frac{4}{m^2 n^2} \xi_j^2 \xi_k^2 \quad (j, k = 1, 2, 3; m, n > 0).\end{aligned}\quad (14)$$

The phases in Eqs. 14 are as large as ϕ_{jk}^{0n} (in Eqs. 13) in magnitudes and the interference terms are increasingly suppressed by factors $\sim \mathcal{O}(\xi^4)$. Hence these interference terms provide very little contribution to the probability in Eq. 10. Both Eqs. 13 and 14 justify our choice of considering only upto $n = 2$ KK neutrinos in the analysis.

In presence of matter, the oscillation probability gets modified after taking into account the charged and neutral current interactions experienced by neutrino. In matter the proba-

bility is determined by the following evolution equation [31].

$$i \frac{d}{dt} \nu'_{jL} = \left[\frac{1}{2E} M_j^\dagger M_j \nu'_{jL} + \sum_{k=1}^3 \begin{pmatrix} Y_{jk} & 0_{1 \times n} \\ 0_{n \times 1} & 0_{n \times n} \end{pmatrix} \nu'_{jL} \right]_{n \rightarrow \infty} \quad \text{with } Y_{jk} = \sum_{\alpha=e,\mu,\tau} U_{\alpha j}^* U_{\alpha k} (\delta_{\alpha e} V_{\text{CC}} + V_{\text{NC}}). \quad (15)$$

The basis are given by Eqs. 4. The charged and neutral current potentials are given by $V_{\text{CC}} = \sqrt{2} G_F n_e$ and $V_{\text{NC}} = -(1/\sqrt{2}) G_F n_n$, where $n_e(n_n)$ are the electron (nucleon) number density along the path of neutrino propagation.

We implement the physics of LED and the oscillation probability in the General Long Baseline Experiment Simulator (GLOBES) [54, 55] (see Appendix for details) and proceed in the following way. Since the impact of LED is perturbative in nature, we require the zero-th KK mode to correspond to the standard mass-squared differences [52]:

$$\Delta m_{kj}^2 = (m_k^0)^2 - (m_j^0)^2 \quad (16)$$

The experimentally measured two standard mass-squared differences Δm_{21}^2 and Δm_{31}^2 help us (using Eqs. 6 and 16) to fix two of the independent Dirac masses m_i^D . Choosing the lightest Dirac mass m_0 to be a free parameter of the LED model, all three Dirac masses m_i^D can then be determined. Clearly for the NH scenario, $m_0 = m_1^D$ and for IH $m_0 = m_3^D$. Once all the three Dirac masses are estimated, we use Eq. 6 to obtain the neutrino masses m_i^n for higher KK modes ($n > 0$). We then use Eq. 10 to determine the oscillation probability with m_0 and R_{ED} as the additional model parameters in addition to the six standard oscillation parameters. We have considered upto two KK modes (*i.e.*, upto $n = 2$) and have checked that the changes in oscillation probability is negligible for higher KK modes.

It needs to be mentioned that there exists a phenomenological constraint on R_{ED} [36]. From Eq. 7, for the zero-mode mass $R_{\text{ED}} m_k < 1/2$ ($k = 1, 2, 3$). But since,

$$m_k^2 = m_j^2 + \Delta m_{kj}^2 \geq \Delta m_{kj}^2, \quad (17)$$

we can write,

$$R_{\text{ED}} \leq \frac{1}{2\sqrt{\Delta m_{kj}^2}} \quad k, j = 1, 2, 3 \text{ and } k \neq j \quad (18)$$

The largest such mass-squared difference is the atmospheric mass-squared difference and is around $2.5 \times 10^{-3} \text{ eV}^2$ (which is Δm_{31}^2 for NH, and Δm_{23}^2 for IH). Thus the physically allowed values of R_{ED} should satisfy,

$$R_{\text{ED}} \leq \frac{1}{2\sqrt{2.5 \times 10^{-3}}} \text{ eV}^{-1} \lesssim 2 \mu\text{m}. \quad (19)$$

3 Probabilities in presence of LED

In Fig. 1 we plot $P(\bar{\nu}_\mu \rightarrow \bar{\nu}_e)$, $P(\bar{\nu}_\mu \rightarrow \bar{\nu}_\mu)$ and $P(\bar{\nu}_\mu \rightarrow \bar{\nu}_\tau)$ as a function of E for both the standard (std) and LED case at the DUNE baseline of 1300 km. The black curves correspond to the standard case. The red (blue) curves show the LED case with the LED parameter as $m_0 = 0$ ($m_0 = 0.05 \text{ eV}$). The compactification radius R_{ED} is $0.5 \mu\text{m}$ for all the LED cases.

Parameter	Best-fit-value	3σ interval	1σ uncertainty
θ_{12} [Deg.]	34.3	31.4 - 37.4	2.9%
θ_{13} (NH) [Deg.]	8.53	8.13 - 8.92	1.5%
θ_{13} (IH) [Deg.]	8.58	8.17 - 8.96	1.5%
θ_{23} (NH) [Deg.]	49.3	41.2 - 51.4	3.5%
θ_{23} (IH) [Deg.]	49.5	41.1 - 51.2	3.5%
Δm_{21}^2 [eV ²]	7.5×10^{-5}	$[6.94 - 8.14] \times 10^{-5}$	2.7%
Δm_{31}^2 (NH) [eV ²]	2.55×10^{-3}	$[2.47 - 2.63] \times 10^{-3}$	1.2%
Δm_{31}^2 (IH) [eV ²]	-2.45×10^{-3}	$-[2.37 - 2.53] \times 10^{-3}$	1.2%
δ_{13} (NH) [Rad.]	-0.92π	$[-\pi, -0.01\pi] \cup [0.71\pi, \pi]$	—
δ_{13} (IH) [Rad.]	-0.42π	$[-0.89\pi, -0.04\pi]$	—

Table 1: The values of the standard oscillation parameters and their uncertainties used in our study. The values were taken from the global fit analysis in [3, 4]. If the 3σ upper and lower limit of a parameter is x_u and x_l respectively, the 1σ uncertainty is $(x_u - x_l)/3(x_u + x_l)\%$ [25].

The solid (dashed) curves in a panel depict the case of NH (IH), and the top (bottom) row shows the case of neutrino (antineutrino). We note that the presence of LED has a two-fold effect: Firstly they introduce new frequencies (driven by the interferences between the standard *i.e.*, zero mode masses and *i.e.*, $n > 0$ KK mode masses) leading to small wiggles in the probability². Secondly, LED decreases the magnitude of the probability (since the SM neutrinos can oscillate into the KK modes). This reduction in magnitude is more for higher values of m_0 . Both of these effects are more prominent at higher energies ($E \gtrsim 6$ GeV).

The overall reduction of probability is mainly due to the correction introduced by terms proportional to $(V_j^0)^2(V_k^0)^2$ (see Eq. 12). The phase differences ϕ_{jk}^{0n} (with $(j, k = 1, 2, 3); (n > 0)$) introduced by the $n > 0$ KK modes (see Eq. 13 and the relevant discussions) are very large compared to the ones induced by the standard ($n = 0$ KK mode) mass-squared differences. Thus the interference terms involving the phase differences $\phi_{jk}^{0n} = \Delta(m_{jk}^{0n})^2 L/2E$ get averaged out. At low E , clearly such terms have high frequencies leading to a complete averaging out. But the frequencies decrease slightly at higher energies which leads to partial non-averaging of the lowest KK mode. Thus the LED effect becomes more apparent at higher energies giving rise to small oscillations/wiggles in the probability spectra. Detailed analytical explanations of such reduction in probability in presence of LED have also been discussed previously, for *e.g.*, in [17].

The impacts of LED are clearly more prominent for the $\nu_\mu \rightarrow \nu_\mu$ channel (second column). The results in this channel neither depend upon $\nu_\mu \rightarrow \nu_\mu$ or $\bar{\nu}_\mu \rightarrow \bar{\nu}_\mu$ channel nor on the

²Presence of the n -th KK mode introduces mass-squared difference $\sim \mathcal{O}(n^2 \times 0.16)$ eV² (see Eq. 13), - which introduces rapid small oscillations on top of the standard oscillations in the probability spectra. But such fast oscillations are not observable due to the finite energy resolution of the detectors. So, in practice it is more realistic to show the somewhat smoothened oscillations after applying the low pass filter in GLOBES with a filter value equal to 125 MeV, - same as the bin widths we will use later for the event spectra and subsequent statistical analysis. But even after such a smoothening, the secondary oscillations due to the KK modes show up as small wiggles which can be observed in principle.

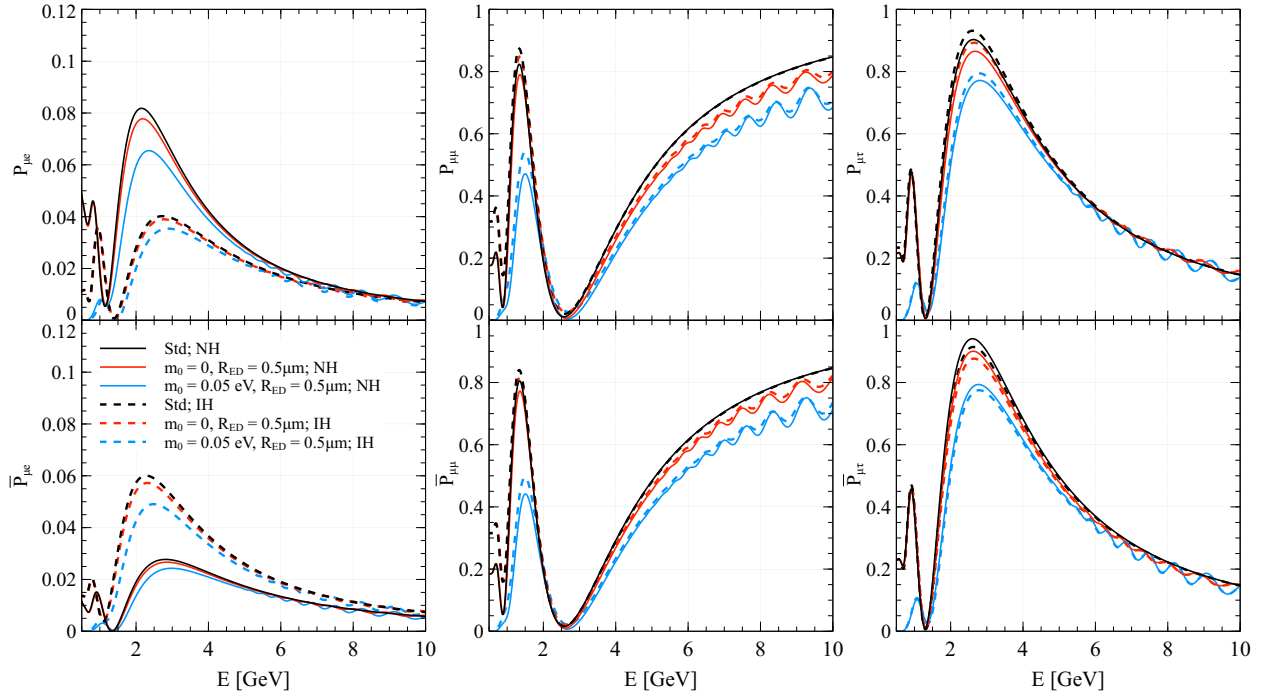


Figure 1: This shows the probabilities as functions of energy (E) for both standard (std.) scenario and in presence of LED at the DUNE FD baseline of 1300 km. The three columns show the cases of the three channels $\nu_\mu \rightarrow \nu_e$, $\nu_\mu \rightarrow \nu_\mu$ and $\nu_\mu \rightarrow \nu_\tau$, while the top (bottom) row depict the case of neutrinos (antineutrinos). The black curves correspond to the std. case while the red and blue curves illustrate the presence of LED (with two different values for the LED parameter m_0 as shown in the figure legend). The LED compactification radius R_{ED} is chosen as $0.5 \mu\text{m}$ for the LED case. The values of all standard oscillation parameters were chosen from Table 1. The solid (dashed) curves correspond to NH (IH).

neutrino mass hierarchy. On the other hand, For $P(\nu_\mu \rightarrow \nu_e)$ ($P(\bar{\nu}_\mu \rightarrow \bar{\nu}_e)$), when going to from IH from NH, the values of probabilities for both std. and LED case are reduced (increased) considerably by roughly a factor 2 – 3. Additionally we also see a slight increase (decrease) of probability in the $\nu_\mu \rightarrow \nu_\tau$ ($\bar{\nu}_\mu \rightarrow \bar{\nu}_\tau$) channel and when changing mass hierarchy from NH to IH.

4 Beam tunes and event spectra

Our goal is to probe the difference between the standard and LED scenario in order to explore the LED parameter space. For generating the events in the two cases, we carry out simulations using GLoBES. The most recent configuration files from the Technical Design Report (TDR) of DUNE [43] have been used in our simulations. DUNE consists of an on-axis 40 kiloton (kt) liquid argon FD housed at the Homestake Mine in South Dakota with a baseline of $L = 1300$ km. A near detector (ND) with target mass 0.067 kt will be installed at a baseline 0.570 km at the Fermi National Accelerator Laboratory (FNAL), in Batavia, Illinois. We use the following broad-band beam tunes :

- The standard low energy (LE) beam tune used in DUNE TDR [25].
- The medium energy (ME) beam tune optimized for ν_τ appearance [25, 26].

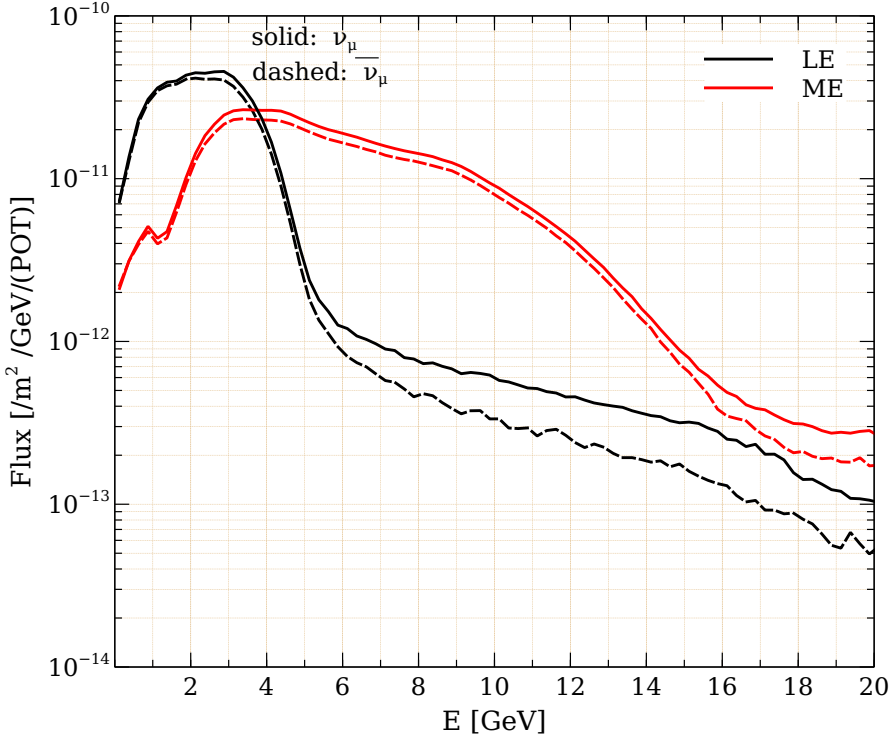


Figure 2: This shows the standard low energy (LE) muon neutrino beam (black) and the (ν_τ -optimized) medium energy-tuned muon neutrino beam (red) at DUNE [25]. The solid (dashed) curves correspond to the beam in ν ($\bar{\nu}$) mode.

Both the beams are produced by a 120 GeV proton beam impinging on a graphite target (delivering 1.1×10^{21} protons on target per year) and are obtained from G4LBNF, a GEANT4 based simulation [56, 57] of the long baseline neutrino facility (LBNF) beamline [25]. The hadrons produced in the graphite target are then focussed using three magnetic horns operated with 300 kA current and are allowed to decay in a helium-filled decay pipe of length 194 m to produce the LE flux. The higher energy tuned ME flux is simulated by replacing the three magnetic horns with two NuMI-like parabolic horns with the second horn starting 17.5 m downstream from the start of the first horn. For both the fluxes, the focusing horns can be operated in forward and reverse current configurations to produce beams in ν and $\bar{\nu}$ modes respectively. The two beam tunes used in our study are shown in Fig. 2. The LE beam (black curve) peaks relatively sharply around $\sim 2 - 3$ GeV and falls rapidly beyond roughly 4 GeV. The ME flux on the other hand peaks around $\sim 3 - 5$ GeV (with a *broad* peak) and falls much slowly thereby retaining significantly higher flux of neutrinos (antineutrinos) compared to the LE beam at $E \gtrsim 4$ GeV. In Fig. 3, we show the event spectra for both std. case and in presence of LED at DUNE FD generated using either the LE beam (red) or ME beam (blue) with a total runtime of 13 years (6.5 yrs. each in ν and $\bar{\nu}$ mode) corresponding to an exposure of 624 kt.MW.yrs. As expected from Fig. 1 and the relevant discussions in Sec. 3, the events show a decrease in presence of LED. and the degree of this decrease is more for ν_μ -like events. Though the event spectra simulated using the LE beam (red) is higher at lower energies, the spectra using the ME beam (blue) takes over at higher energies ($E \gtrsim 3.5$ GeV for ν_e spectra, and $E \gtrsim 2.5$ GeV for ν_μ spectra). This observation

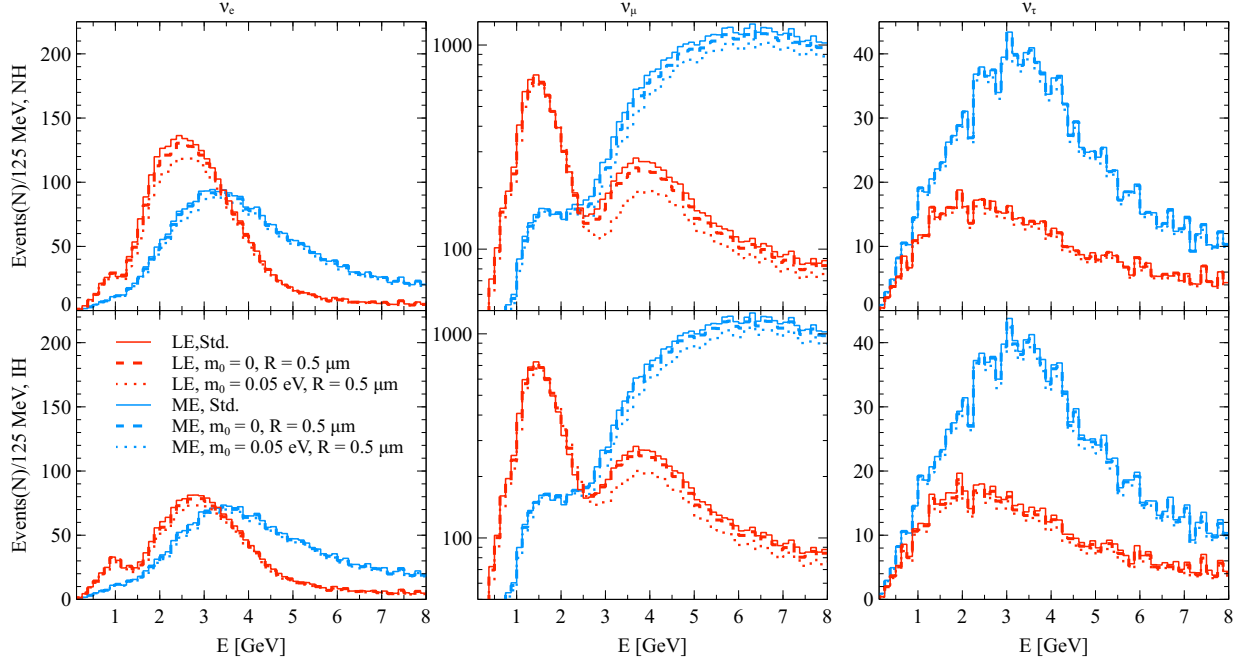


Figure 3: This shows the event spectra generated at DUNE FD, using either the standard LE beam (red) or the ME beam (blue) with a total of 13 yrs. of runtime (6.5 yrs. each in ν and $\bar{\nu}$ mode). The top (bottom) row corresponds to NH (IH). The solid curves correspond to the standard three neutrino scenario, while the thick dashed and the thin dotted curves correspond to the LED case with different sets of the choice of parameters (m_0, R_{ED}) as shown in the legend. The three columns correspond to the ν_e -like, ν_μ -like and ν_τ -like events respectively. Note that the vertical axes of the second column (ν_μ events) are in logarithmic scale for ease of comparison between the events generated by LE and ME beams.

is especially significant for the ν_μ events, - increasing the number of events by more than an order of magnitude when using the ME beam. For *e.g.*, the number of ν_μ events (both for the std. case and in presence of LED) with LE beam lie approximately within 40 – 80 around 8 GeV. But with the ME beam, these numbers can shoot up to around 900 – 1000 at 8 GeV. Since the value of $P(\nu_\mu \rightarrow \nu_\mu)$ is high (close to 1) at higher energies (see Fig. 1), the use of the ME beam (which is expected to offer more statistics at high energies, - see Fig. 2) is thus particularly advantageous for the $\nu_\mu \rightarrow \nu_\mu$ channel. Such a huge statistics at energies beyond 4 GeV is thus expected to offer more sensitivities in probing the effects of LED. For the $\nu_\mu \rightarrow \nu_e$ channel, the number of events N with the LE beam at $E \gtrsim 4$ GeV is very small (for *e.g.*, $N \simeq 5 - 10$ around 8 GeV for NH: left-top panel of Fig. 3) owing to the sharply falling LE flux. But ME beam offers high statistics at higher energy, - thus increasing the number of events to around 20-60 in the range 4-8 GeV for NH. Since the ME beam is already optimized for $\nu_\mu \rightarrow \nu_\tau$ appearance events, the number of ν_τ events is significantly higher compared to the case when LE beam is used. For *e.g.*, in the NH case (top-right panel of Fig. 3) the number of ν_τ events at the peak of the spectrum when using LE is around 16 ($E \simeq 2$ GeV). But using ME beam, the number of ν_τ events at the peak is around 40 ($E \simeq 3$ GeV).

To analyse the role of ME more in probing the physics of LED, we now define the following quantification of difference of event spectra,

$$\Delta N_{\alpha\beta} = |N_{\alpha\beta}^{\text{std}} - N_{\alpha\beta}^{\text{LED}}|, \quad (20)$$

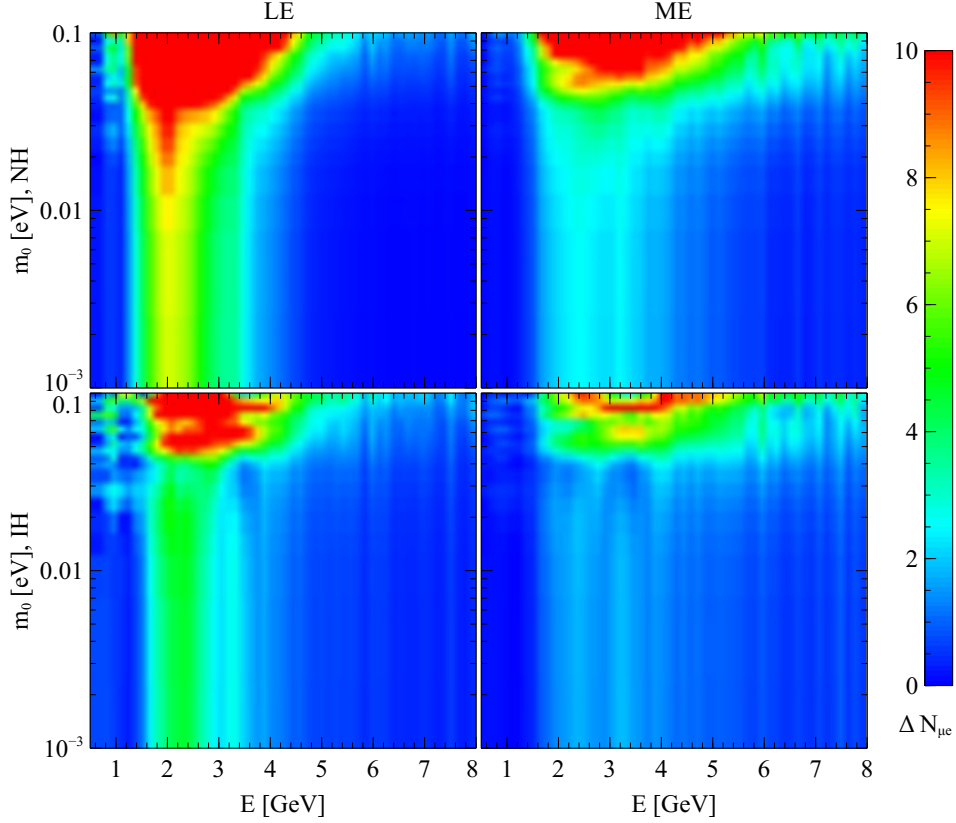


Figure 4: This shows the heatplot for the absolute difference of ν_e -like events for the standard and LED case: $\Delta N_{\mu e} = |N_{\mu e}^{\text{std}} - N_{\mu e}^{\text{LED}}|$ in the plane of m_0 and E . The left (right) column corresponds to the use of LE (ME) beam for the full 13 yrs. of runtime, while the top (bottom) row indicates NH (IH). The best-fit values of the standard oscillation parameters (Table 1) were used in generating this figure.

where the first and second term in the right hand side denote the number of events for the standard and LED case respectively. Clearly the quantity $\Delta N_{\alpha\beta}$ is a function of energy. We estimate $\Delta N_{\alpha\beta}$ for all the energy bins upto 8 GeV at the DUNE FD using either the LE beam or the ME beam alone and generate a heatplot for $\Delta N_{\alpha\beta}$ by varying the lightest neutrino mass m_0 in the range $[0.001, 0.1]$ eV. The LED radius R_{ED} is kept fixed at $0.5 \mu\text{m}$ throughout. Such heatplots are shown in Figs. 4, 5 and 6 for the ν_e, ν_μ and ν_τ events respectively. Clearly, when using LE beam, the deviation of events from the std. case in presence of LED is maximum around $1.5 - 4$ GeV approximately, where the deviation $\Delta N_{\mu e}$ is quantified to be around $\mathcal{O}(10)$ for $m_0 \gtrsim 0.04$ eV (top-left panel of Fig. 4). At higher energies ($\gtrsim 6$ GeV) $\Delta N_{\mu e}$ reduces to very small numbers close to zero. Using ME, the deviation $\Delta N_{\mu e}$ shows a slightly smaller magnitude at lower energies, while maintaining some non-zero value (albeit small and $\sim \mathcal{O}(1)$) at $5 - 8$ GeV. Qualitatively similar observations can also be inferred for the IH case (bottom row of Fig. 4).

For the $\nu_\mu \rightarrow \nu_\mu$ channel, using the ME beam shows a clear significant advantage over the LE beam. This is evident from Fig. 5 for a significantly wide range of energies (approximately 3.5-8 GeV) where the deviation $\Delta N_{\mu\mu}$ can attain high values unlike the case where only LE was used. We note that for a large number of energy bins (with $4.5 \lesssim E \lesssim 7$ GeV), the use of ME beam can easily give $\Delta N_{\mu\mu} \sim \mathcal{O}(100)$ for even very small values of m_0 upto 0.001 eV (top right panel of Fig. 5). In contrast, with the LE beam $\Delta N_{\mu\mu}$ is much smaller for most

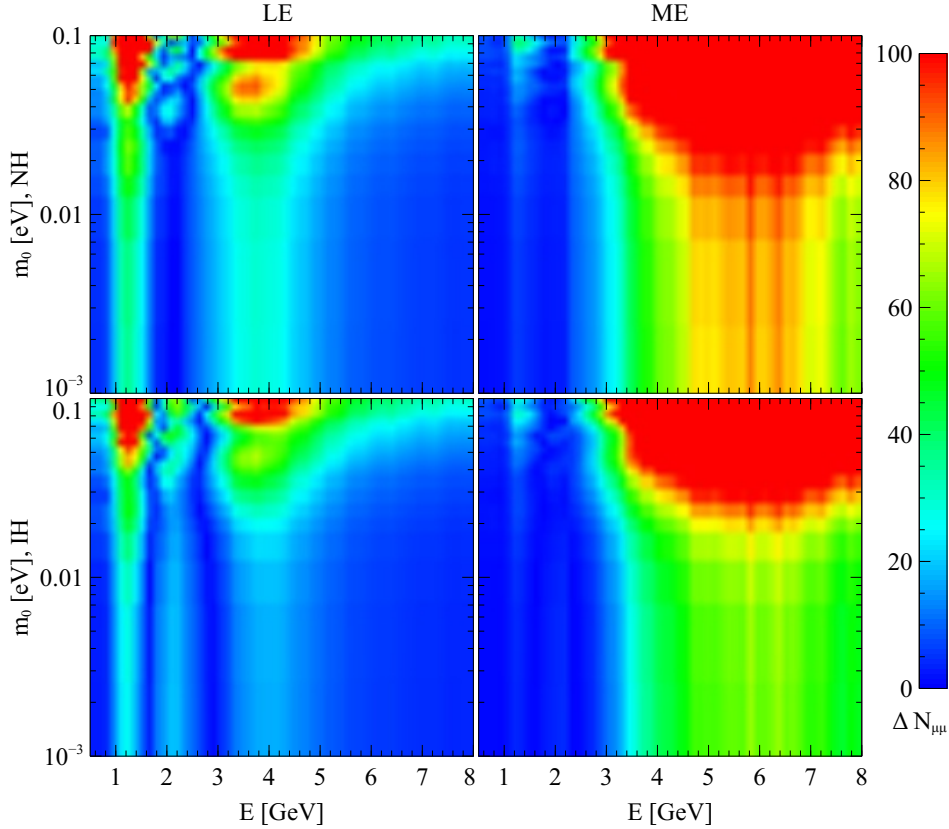


Figure 5: Similar to Fig. 4 but for the ν_μ -like events.

of the energy bins and can reach $\mathcal{O}(100)$ only for very high m_0 ($\gtrsim 0.07$ eV) and only at a relatively narrow energy windows around 4 GeV and 1.5 GeV.

Due to large backgrounds, the efficiencies for detecting ν_τ events at DUNE FD are small. The capability to differentiate between the std. and LED events are also not very good for the ν_τ events. Hence $\Delta N_{\mu\tau}$ can reach only upto $\mathcal{O}(1)$ at best, as observed in Fig. 6. This can be obtained only for high values of m_0 ($\gtrsim 0.06$ eV), and the ME beam may offer only a slight advantage.

5 Analysis methodology

We explore DUNE's capability to probe the LED parameter space by performing a $\Delta\chi^2$ analysis. We use GLoBES [54, 55] for the $\Delta\chi^2$ analysis, using the latest GLoBES configuration files corresponding to the Technical Design Report (TDR) by the DUNE collaboration [43]. This analysis was performed at DUNE FD, after taking into account the rate-based constraints at ND (without explicitly simulating the ND) [35]. Electron neutrino appearance signals (CC), muon neutrino disappearance signals (CC), as well as neutral current (NC) backgrounds and tau neutrino appearance backgrounds (along with the corresponding systematics/efficiencies etc.) are already included in the configuration files. In the present analysis, in addition to events from $\nu_\mu \rightarrow \nu_e$ and $\nu_\mu \rightarrow \nu_\mu$ channels, we consider the $\nu_\mu \rightarrow \nu_\tau$ channel. Charged current interaction of an incoming ν_τ produces a τ lepton, which decays

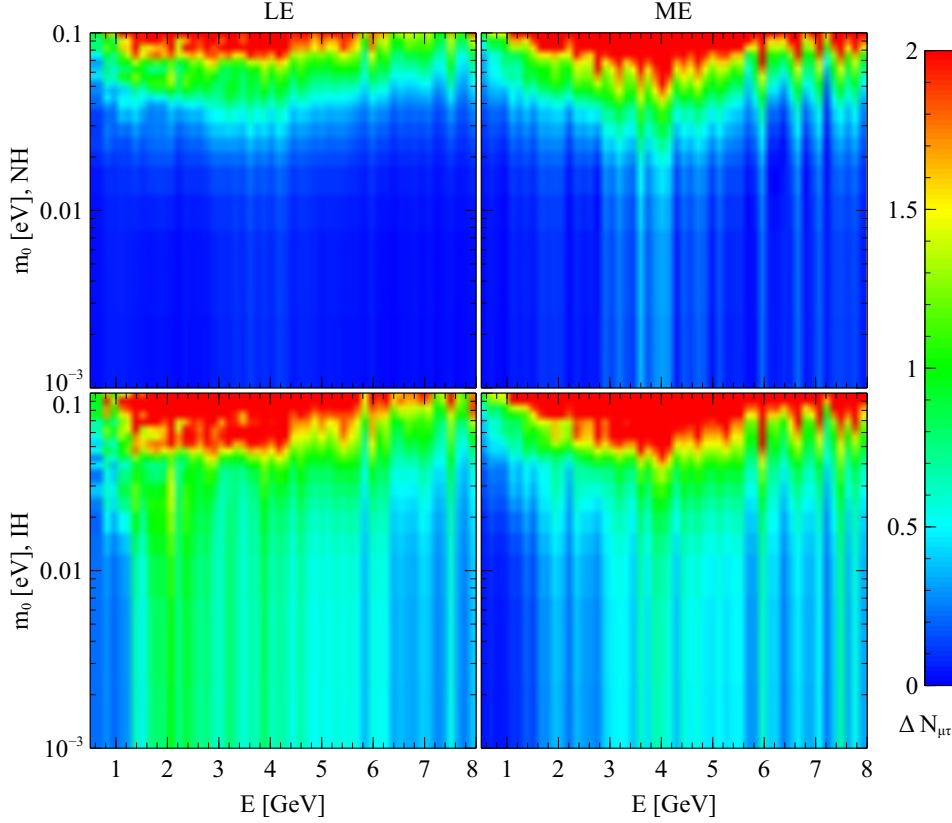


Figure 6: Similar to Figs. 4 and 5 but for the ν_τ -like events.

hadronically (with a branching fraction $\sim 65\%$) or leptonically (with a branching fraction of $\sim 35\%$). The analysis of the hadronic decay channel involves the capability of the detector to study the resulting pions and kaons as well separating NC neutrino background. Following [58], we have used an efficiency to identify 30% hadronically decaying τ events. On the other hand, the leptonic decay channels of τ ($\tau^- \rightarrow e^- \bar{\nu}_e \nu_\tau$; $\tau^- \rightarrow \mu^- \bar{\nu}_\mu \nu_\tau$) are more difficult to analyse, due to the large background mainly consisting of ν_e -CC and ν_μ -CC respectively (along with backgrounds from NC and contaminations due to wrong sign leptons.). Following [59], we have taken 15% efficiency to detect ν_τ events for leptonically decaying τ lepton. We acknowledge that our implementation of the ν_τ channel as a signal is conservative in nature. Nevertheless, this provides a small but non-negligible statistics in terms of events and $\Delta\chi^2$ sensitivity (see Sec. 6). Using a much more sophisticated analysis of ν_τ appearance channel at DUNE (for instance, by implementing jet- clustering algorithms and machine learning techniques, as has been discussed in [60]), one certainly expects to exploit the capabilities of ν_τ appearance channel further. ν_τ interaction cross-sections are set to zero in the original GLoBES TDR configuration files. We include the non-zero ν_τ cross-sections from a slightly older GLoBES configuration [61] and also use new *rules* for ν_τ channel signals in GLoBES following the discussions above.

Below we discuss in detail about the approximate analytical form of the $\Delta\chi^2$ and its

various terms.

$$\Delta\chi^2(\bar{p}^{\text{fit}}) = \min_{(p^{\text{fit}} - \bar{p}^{\text{fit}}; \eta)} \left[\underbrace{2 \sum_x \sum_j \sum_i^{\text{mode channel bin}} \left\{ N_{ijxy}^{\text{LED}}(p^{\text{fit}}; \eta) - N_{ijxy}^{\text{std}}(p^{\text{data}}) + N_{ijxy}^{\text{std}}(p^{\text{data}}) \ln \frac{N_{ijxy}^{\text{std}}(p^{\text{data}})}{N_{ijxy}^{\text{LED}}(p^{\text{fit}}; \eta)} \right\}}_{\text{statistical}} \right. \\ \left. + \underbrace{\sum_l \frac{(p_l^{\text{data}} - p_l^{\text{fit}})^2}{\sigma_{p_l}^2}}_{\text{prior}} + \underbrace{\sum_k \frac{\eta_k^2}{\sigma_k^2}}_{\text{systematics}} \right], \quad (21)$$

where the index i is summed over the energy bins in the range $0.5 - 18$ GeV³. The index j corresponds to three oscillation channels ($\nu_\mu \rightarrow \nu_e, \nu_\mu \rightarrow \nu_\mu, \nu_\mu \rightarrow \nu_\tau$) while the index x runs over the modes (ν and $\bar{\nu}$). N^{std} (treated as *data*) and N^{LED} (treated as *fit*) are the set of events corresponding to the standard and LED cases respectively. The terms in the first row of the right-hand-side of Eq. (21) correspond to the statistical contribution. The first two terms in the statistical contribution to the $\Delta\chi^2$ constitute the algebraic difference ($N^{\text{LED}} - N^{\text{std}}$) while the last term (*i.e.*, the logarithmic-term) corresponds to the fractional difference between the two sets of events⁴. Note that p^{data} ($\{\theta_{12}, \theta_{13}, \theta_{23}, \delta_{13}, \Delta m_{21}^2, \Delta m_{31}^2\}$) and p^{fit} ($\{\theta_{12}, \theta_{13}, \theta_{23}, \delta_{13}, \Delta m_{21}^2, \Delta m_{31}^2, m_0, R_{\text{ED}}\}$) refer to the set of oscillation parameters for the calculation of N^{std} and N^{LED} respectively. *Data* (*i.e.*, N^{std}) is generated for the standard three-neutrino case by considering the best-fit values of the oscillation parameters from Table 1. The events in the LED case (N^{LED}) are then fit to the *data* by varying the set of LED parameters $\bar{p}^{\text{fit}} : \{m_0, R_{\text{ED}}\}$. The set of standard oscillation parameters ($p^{\text{fit}} - \bar{p}^{\text{fit}}$) are also varied in the *fit* (using the uncertainties listed in Table 1).

The two terms in the second line of Eq. 21 correspond to the prior and systematics respectively. The *prior* term accounts for the penalty of the l number of *fit* parameters deviating away from the corresponding p^{data} . The degree of this deviation is controlled by σ_{p_l} which is the uncertainty in the prior measurement of the best-fit values of p^{data} (see the last column of Table 1 for the values used in the present analysis). The *systematics*-term accounts for the variation of the systematic/nuisance parameters. η is the set of values of k -systematics parameters $\{\eta_1, \eta_2, \dots, \eta_k\}$ while σ_k is the uncertainty in the corresponding systematics.

This way of treating the nuisance parameters in the $\Delta\chi^2$ calculation is known as the *method of pulls* [62–65]. Regarding the systematics [43], the ν_e and $\bar{\nu}_e$ signal modes have a normalization uncertainty of 2% each, whereas the ν_μ and $\bar{\nu}_\mu$ signals have a normalization uncertainty of 5% each. The ν_τ and $\bar{\nu}_\tau$ signals have a normalization uncertainty of 20% each. The background normalization uncertainties lie within 5% – 20% and include correlations among various sources of background (coming from beam $\nu_e/\bar{\nu}_e$ contamination,

³We have a total of 66 energy bins in the range $0.5 - 18$ GeV: 60 bins each having a width of 0.125 GeV in the energy range of $0.5 - 8$ GeV and 6 bins with variable widths beyond 8 GeV [43].

⁴Note that the definition of $\Delta\chi^2$ described in Eq. 21 is Poissonian in nature. In the limit of large events, this reduces to the Gaussian form :

$$\lim_{N \rightarrow \infty} \Delta\chi^2(\bar{p}^{\text{fit}}) \simeq \min_{(p^{\text{fit}} - \bar{p}^{\text{fit}}; \eta)} \left[\sum_x \sum_j \sum_i^{\text{mode channel bin}} \frac{\left(N_{ijxy}^{\text{LED}}(p^{\text{fit}}; \eta) - N_{ijxy}^{\text{std}}(p^{\text{data}}) \right)^2}{N_{ijxy}^{\text{std}}(p^{\text{data}})} + \text{prior} + \text{systematics} \right].$$

flavour misidentification, NC and ν_τ). The final estimate of the $\Delta\chi^2$ as a function of the set of desired parameters (\bar{p}^{fit}) (*i.e.*, as a function of the LED parameters m_0 and R_{ED}) for a given set of fixed parameters p^{data} is obtained after minimizing the entire quantity within the square bracket in Eq. 21 over the relevant set of rest of the *fit* parameters $p^{\text{fit}} - \bar{p}^{\text{fit}}$ (*i.e.*, over all the standard oscillation parameters), as well as over the systematics η . This minimization is also referred to as marginalization over the set $\{p^{\text{fit}} - \bar{p}^{\text{fit}}; \eta\}$. Technically, this procedure is the frequentist method of hypotheses testing [63, 66].

6 Results

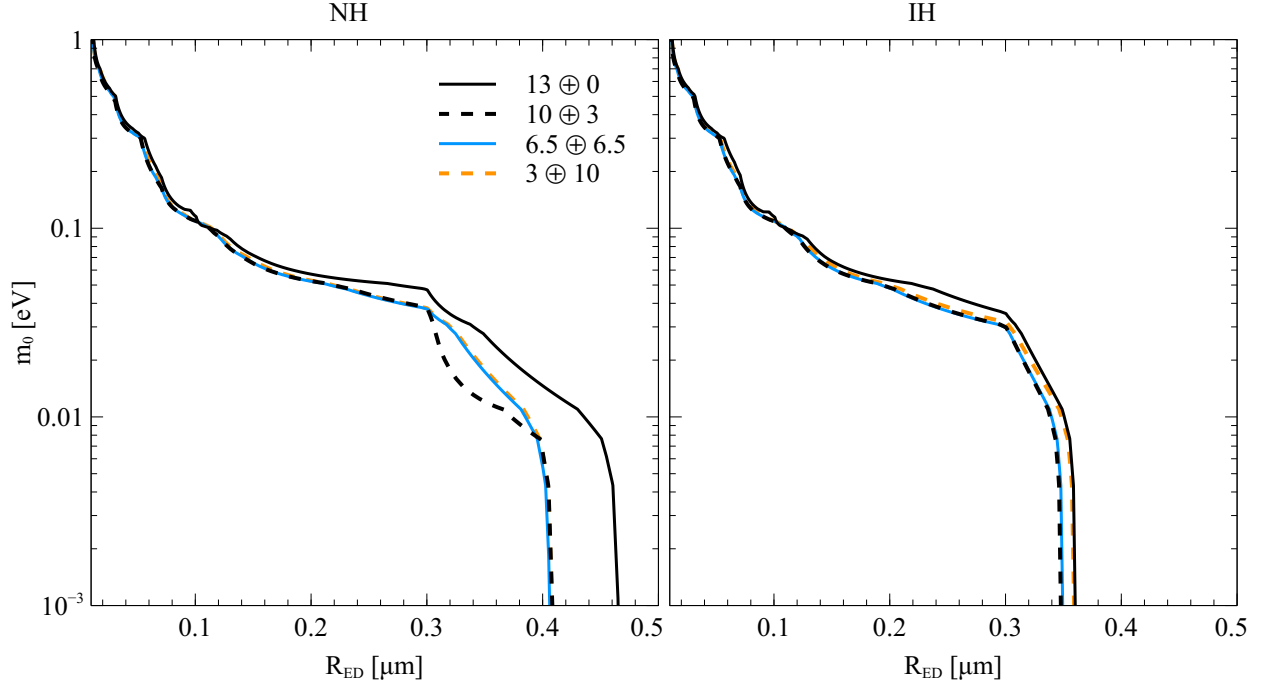


Figure 7: This shows $\Delta\chi^2$ contours at 90% confidence level (C.L.) obtained at DUNE FD at in the parameter space of $m_0 - R_{\text{ED}}$ for various combinations of LE and ME beam. The legends show the runtime combinations (in yrs.) used for LE and ME beams. For *e.g.*, the black solid curve corresponds to 13 yrs. of runtime in LE only; the black dashed curve refers to 10 yrs. of runtime in LE beam combined with 3 yrs. of runtime using ME beam. Runtime in each beam are equally distributed into ν and $\bar{\nu}$ modes. The left (right) columns indicates the case of NH (IH).

From the discussions in Sec. 4, we anticipate that at higher energies, ME beam should give more sensitivity to LED parameters, while the sensitivities at lower energy are expected to be better using the LE beam. In order to properly utilize the entire energy range, we seek to optimize the combinations of runtime using LE and ME beams together. In Fig. 7, we show the 90% C.L. $\Delta\chi^2$ contours (*i.e.*, $\Delta\chi^2 = 4.61$ at two degrees of freedom) in the parameter space of $m_0 - R_{\text{ED}}$ at DUNE FD for different combinations of runtime (in yrs.) using LE and ME beam together such that the total runtime remains fixed at 13 yrs. We marginalise over all six standard oscillation parameters $\theta_{12}, \theta_{13}, \theta_{23}, \delta_{13}, \Delta m_{21}^2, \Delta m_{31}^2$ by varying the value of θ_{23} to include both the octants and assuming the neutrino mass hierarchy to be either NH or IH at a time. We take the prior uncertainties of the oscillation parameters as tabulated in

Table 1 with δ_{13} allowed to vary over the entire range of $[-\pi, \pi]$. From Fig. 7, we note that the use of ME beam even for a small runtime increases the sensitivity to LED parameters in comparison to LE beam alone, especially for the NH scenario (left panel of Fig. 7). For *e.g.*, for $m_0 \simeq 0.001$ eV, DUNE can exclude $R_{\text{ED}} \gtrsim 0.47 \mu\text{m}$ with LE beam alone. But using a combination of LE + ME beam, the exclusion capability becomes stronger by almost 13% ($R_{\text{ED}} \gtrsim 0.41 \mu\text{m}$). The role of the ME beam is most significant in the region $m_0 \lesssim 0.01$ eV. For values of $m_0 (\gtrsim 0.1 \text{ eV})$, all the combinations (including the LE beam alone) give similar sensitivities. For the IH scenario, the sensitivity with LE alone is already better ($R_{\text{ED}} \gtrsim 0.36 \mu\text{m}$ at $m_0 \simeq 0.001$ eV) than the NH case. Sharing more than half of the total runtime with the ME beam offers a slight improvement of the bounds (by a factor of 5 – 6% roughly). But a smaller runtime with the ME beam does not practically offer improvement compared to running the experiment with LE beam alone (orange dashed curve in the right panel of Fig. 7). Similar to the NH case, the role of the ME beam is not relevant above $m_0 \simeq 0.1$ eV. From Fig. 7, it appears that a runtime combination of $(10 \oplus 3)$ yrs. in the $(\text{LE} \oplus \text{ME})$ beam combination offers the best optimized combination to probe the LED parameter space for both NH and IH scenario. It needs to be mentioned that all the sensitivities to R_{ED} are approximately independent of m_0 for $m_0 \lesssim 0.01$ eV. Below we compare the results of this optimized combination in more detail.

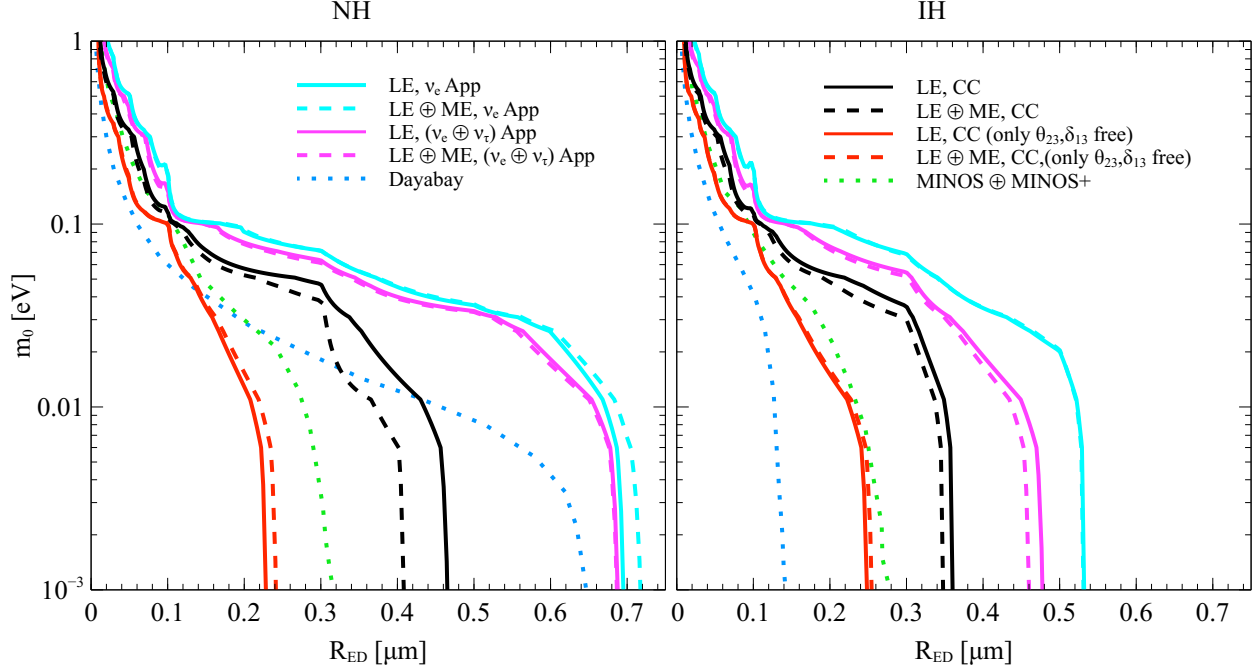


Figure 8: This shows 90% C.L. $\Delta\chi^2$ contours obtained with DUNE FD in the parameter space of $m_0 - R_{\text{ED}}$. The solid curves show the results with LE beam alone (13 yrs. of runtime), while the dashed curves show the results when the optimized runtime combination of 10 yrs. with LE beam was used in conjunction with 3 yrs. with ME beam. The cyan and magenta curves depict the case when ν_e appearance channel and $(\nu_e + \nu_\tau)$ appearance channel was used respectively for the analysis. The black curves show the results when all three CC channels (ν_e appearance, ν_τ appearance and ν_μ disappearance) were used together. For the cyan, magenta and black curves, all six standard oscillation parameters were considered free and marginalized over. The red curves depict the results when only two standard oscillation parameters θ_{23} and δ_{13} were marginalized while the rest were kept fixed at their bestfit values (Table 1). The left (right) panel corresponds to the NH (IH) case. The dotted contours refer to the 90% exclusion contours using the dataset of MINOS/MINOS+ (green) and Daya Bay (blue) respectively (as estimated in [36]).

Fig. 8 shows the 90% C.L. $\Delta\chi^2$ contours in the LED parameter space at DUNE FD. It compares the sensitivities obtained from LE beam alone (13 yrs. of runtime) with that obtained from the optimized runtime combination of $(10 \oplus 3)$ yrs. using $(\text{LE} \oplus \text{ME})$ beam together, by analyzing the sensitivities contributed by various oscillation channels. At first we perform a conservative analysis by keeping all six standard oscillation parameters free and marginalizing over all of them (cyan, magenta, black contours in Fig. 8). In the following we discuss various noteworthy observations, by considering the NH scenario first (left panel Fig. 8). The ν_e appearance channel alone can constrain R_{ED} upto roughly $0.69 \mu\text{m}$ for $m_0 = 0.001 \text{ eV}$ when using LE beam only for the NH scenario. Combining this channel with the ME beam actually worsens the sensitivity slightly. Considering ν_τ appearance channel into the analysis proves to be of very small impact as well (whether using LE beam alone or the optimized combination of $\text{LE} \oplus \text{ME}$ beam). Adding the ν_μ disappearance channel using the LE beam alone significantly strengthens the constraints by excluding $R_{\text{ED}} \gtrsim 0.47 \mu\text{m}$, an improvement of roughly 33% over what can be achieved using ν_e appearance channel using LE beam only. We emphasize that this constraint obtained using the latest DUNE TDR configurations and three oscillation channels is slightly better when compared to other projected DUNE constraints [31, 35, 38]. The optimized combination of runtime using $(\text{LE} \oplus \text{ME})$ beams tightens the constraints further by a factor of 13% to a value $R_{\text{ED}} \gtrsim 0.41 \mu\text{m}$ at $m_0 = 0.001 \text{ eV}$ (as already mentioned in the context of Fig. 7.). Use of $\nu_\mu \rightarrow \nu_\mu$ oscillation channel at DUNE begins to offer better sensitivity below $m_0 \lesssim 0.01 \text{ eV}$ than the Daya Bay data.

We also perform the analysis with an optimistic case, - assuming that all the standard oscillation parameters except θ_{23} and δ_{13} will be known to a very high accuracy when the actual data taken by DUNE will be analyzed. In the optimistic scenario we only marginalize over θ_{23} and δ_{13} and keep the rest of the oscillation parameters fixed to their best fit values in the *fit*. We show the consequent sensitivities (taking all three oscillation channels together) as the red lines in Fig. 8. Using LE beam alone, such an analysis puts a strong constraint and excludes $R_{\text{ED}} \gtrsim 0.23 \mu\text{m}$ at $m_0 \simeq 0.001 \text{ eV}$ (an improvement of almost 50% over the corresponding conservative assumption). The optimized combination of $(\text{LE} \oplus \text{ME})$ does not prove to be very beneficial in the optimistic assumption, - rather worsening the exclusion region slightly: $R_{\text{ED}} \gtrsim 0.24 \mu\text{m}$ at $m_0 \simeq 0.001 \text{ eV}$. We should mention that in a very recent analysis of LED parameters using simulated data at DUNE FD with a high energy beam alone where the authors have marginalised over $\delta_{13}, \Delta m_{31}^2, \theta_{23}$ with the octant of θ_{23} fixed, gives a similar constraint at 2σ C.L. [39].

Crucially we observe that with the optimistic assumption DUNE can reach into the sensitivity regions for MINOS/MINOS+ for almost all values of m_0 under consideration. The future projections of other LBL experiments [38] such as T2HK and ESS ν SB give constraints ($R_{\text{ED}} \gtrsim 0.45 \mu\text{m}$ and $R_{\text{ED}} \gtrsim 0.6 \mu\text{m}$ respectively at $m_0 \simeq 0.001 \text{ eV}$) comparable to what the present analysis finds using only LE beam at DUNE. The analyses of Gallium experiments GALLEX [67], SAGE [68], BEST [69] give somewhat weaker bounds on LED and can be well-excluded by DUNE, as well as reactor experiments like Daya Bay. Though the data from the direct neutrino mass measurement experiment KATRIN [42] only constrains LED very weakly, the combined analysis of KATRIN with MINOS/MINOS+ and Daya Bay can give very strong bounds on R_{ED} [36], - which are comparable to what can be achieved using the optimistic assumptions at DUNE. Apart from the neutrino sector, the bounds on LED have also been obtained from tabletop gravitational experiments [70–74], collider

experiments [75–79], and also from astrophysical [80–87] and cosmological data [88–92]. The tabletop experiments give constraints on R_{ED} which are about two orders of magnitude weaker ($R_{\text{ED}} \gtrsim 37 \mu\text{m}$ at 95% C.L.) than what can be achieved at DUNE Using astrophysical data, very strong constraints ranging in $R_{\text{ED}} \gtrsim 0.16 - 916 \text{ nm}$ have been obtained. However, these limits depend on the technique and some assumptions [93] in the analyses.

For the IH scenario (right panel of Fig. 8), the sensitivities obtainable by the ν_e appearance ($R_{\text{ED}} \gtrsim 0.53 \mu\text{m}$) and $(\nu_e \oplus \nu_\tau)$ appearance channels ($R_{\text{ED}} \gtrsim 0.48 \mu\text{m}$) are better compared to the NH case. Consequently the bound achieved with all three CC channels are better than the NH case, even though the contribution from the dominant channel $\nu_\mu \rightarrow \nu_\mu$ is largely insensitive of neutrino mass hierarchy⁵. Further, we note that the combination with ME beam offers only a slight improvement of results, especially for $\nu_\mu \rightarrow \nu_\tau$ and $\nu_\mu \rightarrow \nu_\mu$ channels. Thus the optimistic assumptions increase the sensitivities significantly, in the IH case, by almost 30%. All the constraints obtained on R_{ED} for the lowest m_0 value (0.001 eV) are tabulated together in Table 2.

Neutrino Mass Hierarchy	Marginalization Assumption	Channel	Beam used	Bounds on $R_{\text{ED}} [\mu\text{m}]$ (90% C.L.)
NH	All six std. osc. parameters free	$\nu_\mu \rightarrow \nu_e$	LE	0.69
			LE \oplus ME	0.72
		$(\nu_\mu \rightarrow \nu_e) \oplus (\nu_\mu \rightarrow \nu_\tau)$	LE	0.68
			LE \oplus ME	0.68
		$(\nu_\mu \rightarrow \nu_e) \oplus (\nu_\mu \rightarrow \nu_\tau) \oplus (\nu_\mu \rightarrow \nu_\mu)$	LE	0.47
			LE \oplus ME	0.41
	θ_{23}, δ_{13} free	$(\nu_\mu \rightarrow \nu_e) \oplus (\nu_\mu \rightarrow \nu_\tau) \oplus (\nu_\mu \rightarrow \nu_\mu)$	LE	0.23
			LE \oplus ME	0.24
IH	All six std. osc parameters free	$\nu_\mu \rightarrow \nu_e$	LE	0.53
			LE \oplus ME	0.53
		$(\nu_\mu \rightarrow \nu_e) \oplus (\nu_\mu \rightarrow \nu_\tau)$	LE	0.48
			LE \oplus ME	0.46
		$(\nu_\mu \rightarrow \nu_e) \oplus (\nu_\mu \rightarrow \nu_\tau) \oplus (\nu_\mu \rightarrow \nu_\mu)$	LE	0.36
			LE \oplus ME	0.34
	θ_{23}, δ_{13} free	$(\nu_\mu \rightarrow \nu_e) \oplus (\nu_\mu \rightarrow \nu_\tau) \oplus (\nu_\mu \rightarrow \nu_\mu)$	LE	0.25
			LE \oplus ME	0.26

Table 2: The table shows the bounds on $R_{\text{ED}} [\mu\text{m}]$ (as read off from Fig. 8) beyond which LED is excluded at 90% C.L. for $m_0 \simeq 0.001 \text{ eV}$.

⁵For small m_0 ($\lesssim 0.1 \text{ eV}$), in the NH case we have $\xi_3 \gg \xi_1, \xi_2$. Thus from Eqs. 12 and 13 it is clearly seen that the LED effects on probability in Eq. 10 are dominated by terms when the index j equals 3. But such terms are also multiplied by the PMNS matrix terms such as $|U_{\alpha 3}|^2$ ($\alpha = e, \mu, \tau$). For the $\nu_\mu \rightarrow \nu_e$ channel (as well as in $\bar{\nu}_e \rightarrow \bar{\nu}_e$ channel in reactor neutrino experiments), the very small magnitudes of $|U_{e3}|^2$ thus suppresses the dominant LED terms for NH. But for IH, $\xi_3 \ll \xi_1, \xi_2$, and the corresponding PMNS matrix factors are $|U_{\alpha 1}|^2$ and $|U_{\alpha 2}|^2$, - which are reasonably large for all $\alpha = e, \mu, \tau$. This makes the sensitivity to LED parameters in the $\nu_\mu \rightarrow \nu_e$ channel stronger in the IH case. But due to absence of such suppression by the PMNS matrix terms, the other oscillation channels are mostly independent of neutrino mass hierarchy.

Finally it should be mentioned that explicitly simulating an ND and performing the analysis to a combined dataset at FD and ND should boost the LED constraints considerably. But this demands careful consideration of systematic uncertainties, especially the bin-by-bin shape related systematics and consequently a considerable amount of computing power. This is beyond the scope of the present analysis and we leave it as a future work.

7 Summary and discussions

The LED model was proposed as an elegant solution to the hierarchy problem. It also offers a natural explanation of neutrino mass generation. All the SM particles including the left handed neutrinos lie on the familiar 4-dimensional spacetime known as brane. The brane is embedded within a higher dimensional $(4 + n)$ spacetime (with n extra spatial dimension) known as bulk. All the particles that are singlets under the SM symmetries (such as gravitons, right handed neutrinos) can propagate into the bulk. We consider effectively 1 extra spatial dimension. The couplings of the three right handed neutrino fields lying in the $(4 + 1)$ dimension with the three left handed SM neutrino fields in the 4 dimensional spacetime, are suppressed by the large volume of the extra spatial dimension and generates tiny masses for the active neutrinos in a natural way. The three five dimensional right handed neutrino fields behave like infinite number of Kaluza-Klein (KK) modes from a four-dimensional point of view after the compactification of the fifth dimension. The compactification radius R_{ED} and the lightest Dirac neutrino mass (m_0) (in addition to the six standard oscillation parameters) determine the neutrino oscillation probability in presence of LED.

In the present work we study the capabilities of DUNE FD to probe the LED parameters m_0 and R_{ED} by using combination of different beam tunes. After a brief overview of the theoretical basics of LED in the context of neutrino oscillation (Sec. 2), we analyze the oscillation probability for the three channels $\nu_\mu \rightarrow \nu_e$, $\nu_\mu \rightarrow \nu_\mu$ and $\nu_\mu \rightarrow \nu_\tau$ (Sec. 3). We note the two-fold impact of LED, - namely an overall reduction of the magnitude of oscillation probability for all flavours, and introduction of additional frequencies (due to transition into the KK modes) in the probability spectrum. The impacts of LED seem to be more pronounced at higher energies ($\gtrsim 5$ GeV), which is especially prominent for the $\nu_\mu \rightarrow \nu_\mu$ channel. In Sec. 4, we show the two beams used in the present analysis. The first beam is the standard low energy (LE) tuned neutrino beam at DUNE peaking at low energies (2 – 3 GeV) and falling sharply beyond 4 GeV. The second beam is the ν_τ -optimized beam that has a broad peak at energies (3 – 5 GeV) and falling much slowly beyond that. We compare the event spectra using LE beam or ME beam at-a-time for the three channels both in standard case and in presence of LED, and highlight how the ME beam offers more statistics at higher energies, - a fact which gives order-of-magnitude higher events for the $\nu_\mu \rightarrow \nu_\mu$ channel. We then proceed to generate heatplots of the absolute difference of events (generated using either the LE beam or the ME beam) between the standard and LED case in the space of m_0 and neutrino energy E . The heatplots give a clear idea about how using ME beam is expected to help provide higher difference of events between the standard and LED case at higher energy bins, - thus potentially providing more sensitivities for a large range of values of m_0 .

After a detailed discussion of the $\Delta\chi^2$ methods (Sec. 5) we proceed to discuss our main

results in Sec. 6. At first, we generate the 90% C.L. $\Delta\chi^2$ contours in the plane of $m_0 - R_{\text{ED}}$ by for various combinations of runtimes shared between LE and ME beams in order to optimize the runtime combinations. We find that rather than using the LE beam alone, using a combination of (LE \oplus ME) with (10 + 3) yrs. of runtime gives better sensitivities to the LED parameters for both NH and IH case. We then analyze the contributions of the three oscillation channels to the sensitivities and show how the combination of (LE \oplus ME) beams impacts the channels individually. As expected, we find the role of $\nu_\mu \rightarrow \nu_\mu$ channel to be the most crucial and estimate the bounds on R_{ED} as obtained using LE alone or with a combination of (LE \oplus ME). We also perform an analysis using optimistic assumptions that all the values of the standard oscillation parameters except θ_{23}, δ_{13} will be known to a very high precision when the analysis of the actual DUNE data will take place, and find out that the bounds on R_{ED} strengthens significantly for both NH (by 50%) and IH (by 30%).

A Appendix: Details of implementation of the physics of LED into GLoBES

To implement the physics of LED, we follow the prescription of GLoBES manual (GLoBES version 3.2.18, chapter 8). We copy the relevant parts within the GLoBES source code (from the file `glb_probability.c`) to our main C++ file. The relevant parts that are copied are the following three functions.

1. `int (*glb_set_oscillation_parameters_function)(glb_params p, void* user_data),`
2. `int (*glb_get_oscillation_parameters_function)(glb_params p, void* user_data),`
3. `int (*glb_probability_matrix_function)(double P[3][3], int cp_sign, double E, int psteps, const double *lengths, const double *densities, double filter_sigma, void* user_data).`

The first two of these functions are then used to include the additional oscillation parameters that appear in presence of LED (namely m_0 and R_{ED}) in the GLoBES probability engine. Here we follow the prescription implemented in `example6.c` of the GLoBES example directory. The third function above is used for the actual calculation of oscillation probability using Eq. 10 (which is also written below for clarity).

$$P_{\nu_\alpha \rightarrow \nu_\beta}^{\text{LED}} = \left| \sum_{j=1}^3 \sum_{n=0}^2 U_{\alpha j}^* U_{\beta j} (V_j^n)^2 \exp\left(-i \frac{(m_j^n)^2 L}{2E}\right) \right|^2. \quad (\text{A.1})$$

Note that we have considered the KK modes upto $n = 2$ since the contributions for $n > 2$ is negligible. Here, U is usual 3×3 PMNS mixing matrix, L is the neutrino propagation distance (1300 km) and E is the neutrino energy. To proceed further, we note that expanding Eq. 15 using the matrix form for M in Eq. 3 upto $n = 2$ KK modes, we can arrive at the following equation for neutrino evolution in matter in presence of LED (see Appendix A

of [29] for a detailed calculation).

$$i \frac{d}{dt} \begin{pmatrix} \nu_1^0 \\ \nu_2^0 \\ \nu_3^0 \\ \nu_1^1 \\ \nu_2^1 \\ \nu_3^1 \\ \nu_1^2 \\ \nu_2^2 \\ \nu_3^2 \end{pmatrix} = \frac{1}{2ER_{\text{ED}}^2} \underbrace{\begin{pmatrix} \eta_1 + X_{11} & X_{12} & X_{13} & \kappa_1 & 0 & 0 & 2\kappa_1 & 0 & 0 \\ X_{21} & \eta_2 + X_{22} & X_{23} & 0 & \kappa_2 & 0 & 0 & 2\kappa_2 & 0 \\ X_{31} & X_{32} & \eta_3 + X_{33} & 0 & 0 & \kappa_3 & 0 & 0 & 2\kappa_3 \\ \kappa_1 & 0 & 0 & 1 & 0 & 0 & 0 & 0 & 0 \\ 0 & \kappa_2 & 0 & 0 & 1 & 0 & 0 & 0 & 0 \\ 0 & 0 & \kappa_3 & 0 & 0 & 1 & 0 & 0 & 0 \\ 2\kappa_1 & 0 & 0 & 0 & 0 & 0 & 4 & 0 & 0 \\ 0 & 2\kappa_2 & 0 & 0 & 0 & 0 & 0 & 4 & 0 \\ 0 & 0 & 2\kappa_3 & 0 & 0 & 0 & 0 & 0 & 4 \end{pmatrix}}_{\mathcal{H}} \begin{pmatrix} \nu_1^0 \\ \nu_2^0 \\ \nu_3^0 \\ \nu_1^1 \\ \nu_2^1 \\ \nu_3^1 \\ \nu_1^2 \\ \nu_2^2 \\ \nu_3^2 \end{pmatrix}. \quad (\text{A.2})$$

Here,

$$\begin{aligned} X_{jk} &= 2ER_{\text{ED}}^2 Y_{jk} = 2ER_{\text{ED}}^2 \sum_{\alpha=e,\mu,\tau} U_{\alpha j}^* U_{\alpha k} (\delta_{\alpha e} V_{\text{CC}} + V_{\text{NC}}), \\ \kappa_j &= \sqrt{2}\xi_j = \sqrt{2}m_j^D R_{\text{ED}}, \\ \eta_j &= (N + 1/2)\kappa_j^2, \quad (j, k = 1, 2, 3), \end{aligned} \quad (\text{A.3})$$

such that N is the total number of neutrino mass states upto $n = 2$ KK modes (*i.e.*, $N = 9$). The determination of the matrix V and the mass-squares $(m_j^n)^2$ in Eq. A.1 now boils down to the estimation of eigenvectors and eigenvalues of the mass-basis hamiltonian \mathcal{H} indicated in Eq. A.2. This eigenvalue problem is numerically solved using the C++ package `Armadillo` [94, 95] and estimate the oscillation probability from Eq. A.1. Finally, before returning the probability value from the function `int (*glb_probability_matrix_function)()`, the GLoBES low-pass filter is applied (by passing the filter value from the `glb` file through the variable `double filter_sigma` in order to reduce the fast oscillations that are not observable by the finite energy resolution of the detector. As a final step, the three redefined GLoBES functions mentioned above are registered in the main C++ code by using the function,

```
int glbRegisterProbabilityEngine(int n_parameters,
glb_probability_matrix_function prob_func,
glb_set_oscillation_parameters_function set_params_func,
glb_get_oscillation_parameters_function get_params_func,
void* user_data).
```

This way of including the physics of LED (or any new physics) into GLoBES following the steps prescribed in the manual enables us to use the usual GLoBES commands for the numerical calculation of probability, event spectra and $\Delta\chi^2$.

Acknowledgments

The authors acknowledge support from the grant NRF-2022R1A2C1009686. This research was supported by the Chung-Ang University Research Scholarship Grants in 2023. MM thanks Samiran Roy for helpful discussions regarding LED. MM acknowledges the help of Chang-Hyeon Ha in using the cluster at Chung-Ang University for performing some of the numerical calculations presented in the paper. This work reflects the views of the authors and not those of the DUNE collaboration.

References

- [1] SUPER-KAMIOKANDE collaboration, *Evidence for oscillation of atmospheric neutrinos*, *Phys. Rev. Lett.* **81** (1998) 1562 [[hep-ex/9807003](#)].
- [2] SNO collaboration, *Measurement of the rate of $\nu_e + d \rightarrow p + p + e^-$ interactions produced by ^8B solar neutrinos at the Sudbury Neutrino Observatory*, *Phys. Rev. Lett.* **87** (2001) 071301 [[nucl-ex/0106015](#)].
- [3] P. F. De Salas, D. V. Forero, S. Gariazzo, P. Martínez-Miravé, O. Mena, C. A. Ternes et al., “Chi2 profiles from Valencia neutrino global fit.” <http://globalfit.astroparticles.es/>, 2021. 10.5281/zenodo.4726908.
- [4] P.F. de Salas, D.V. Forero, S. Gariazzo, P. Martínez-Miravé, O. Mena, C.A. Ternes et al., *2020 global reassessment of the neutrino oscillation picture*, *JHEP* **02** (2021) 071 [[2006.11237](#)].
- [5] I. Esteban, M. C. Gonzalez-Garcia, M. Maltoni, I. Martinez-Soler, J. P. Pinheiro and T. Schwetz, “NuFIT 6.0.” www.nu-fit.org, 2024.
- [6] I. Esteban, M.C. Gonzalez-Garcia, M. Maltoni, I. Martinez-Soler, J.a.P. Pinheiro and T. Schwetz, *NuFit-6.0: Updated global analysis of three-flavor neutrino oscillations*, [2410.05380](#).
- [7] F. Capozzi, E. Lisi, A. Marrone and A. Palazzo, *Current unknowns in the three neutrino framework*, *Prog. Part. Nucl. Phys.* **102** (2018) 48 [[1804.09678](#)].
- [8] P. Minkowski, $\mu \rightarrow e\gamma$ at a Rate of One Out of 10^9 Muon Decays?, *Phys. Lett. B* **67** (1977) 421.
- [9] T. Yanagida, *Horizontal gauge symmetry and masses of neutrinos*, *Conf. Proc. C* **7902131** (1979) 95.
- [10] R.N. Mohapatra and G. Senjanovic, *Neutrino Mass and Spontaneous Parity Nonconservation*, *Phys. Rev. Lett.* **44** (1980) 912.
- [11] J. Schechter and J.W.F. Valle, *Neutrino Masses in $SU(2) \times U(1)$ Theories*, *Phys. Rev. D* **22** (1980) 2227.
- [12] N. Arkani-Hamed, S. Dimopoulos and G.R. Dvali, *The Hierarchy problem and new dimensions at a millimeter*, *Phys. Lett. B* **429** (1998) 263 [[hep-ph/9803315](#)].
- [13] I. Antoniadis, N. Arkani-Hamed, S. Dimopoulos and G.R. Dvali, *New dimensions at a millimeter to a Fermi and superstrings at a TeV*, *Phys. Lett. B* **436** (1998) 257 [[hep-ph/9804398](#)].
- [14] N. Arkani-Hamed, S. Dimopoulos and G.R. Dvali, *Phenomenology, astrophysics and cosmology of theories with submillimeter dimensions and TeV scale quantum gravity*, *Phys. Rev. D* **59** (1999) 086004 [[hep-ph/9807344](#)].
- [15] N. Arkani-Hamed, S. Dimopoulos, G.R. Dvali and J. March-Russell, *Neutrino masses from large extra dimensions*, *Phys. Rev. D* **65** (2001) 024032 [[hep-ph/9811448](#)].

- [16] K.R. Dienes, E. Dudas and T. Gherghetta, *Neutrino oscillations without neutrino masses or heavy mass scales: A Higher dimensional seesaw mechanism*, *Nucl. Phys. B* **557** (1999) 25 [[hep-ph/9811428](#)].
- [17] G.R. Dvali and A.Y. Smirnov, *Probing large extra dimensions with neutrinos*, *Nucl. Phys. B* **563** (1999) 63 [[hep-ph/9904211](#)].
- [18] R. Barbieri, P. Creminelli and A. Strumia, *Neutrino oscillations from large extra dimensions*, *Nucl. Phys. B* **585** (2000) 28 [[hep-ph/0002199](#)].
- [19] F. Nortier, *Large star/rose extra dimension with small leaves/petals*, *Int. J. Mod. Phys. A* **35** (2020) 2050182 [[2001.07102](#)].
- [20] DUNE collaboration, *Long-Baseline Neutrino Facility (LBNF) and Deep Underground Neutrino Experiment (DUNE) Conceptual Design Report Volume 2: The Physics Program for DUNE at LBNF*, [1512.06148](#).
- [21] DUNE collaboration, *Long-Baseline Neutrino Facility (LBNF) and Deep Underground Neutrino Experiment (DUNE): Conceptual Design Report, Volume 4 The DUNE Detectors at LBNF*, [1601.02984](#).
- [22] HYPER-KAMIOKANDE PROTO- collaboration, *Physics potential of a long-baseline neutrino oscillation experiment using a J-PARC neutrino beam and Hyper-Kamiokande*, *PTEP* **2015** (2015) 053C02 [[1502.05199](#)].
- [23] HYPER-KAMIOKANDE collaboration, *Physics potentials with the second Hyper-Kamiokande detector in Korea*, *PTEP* **2018** (2018) 063C01 [[1611.06118](#)].
- [24] ESSNUSB collaboration, *A very intense neutrino super beam experiment for leptonic CP violation discovery based on the European spallation source linac*, *Nucl. Phys. B* **885** (2014) 127 [[1309.7022](#)].
- [25] DUNE collaboration, *Deep Underground Neutrino Experiment (DUNE), Far Detector Technical Design Report, Volume II: DUNE Physics*, [2002.03005](#).
- [26] “Dune fluxes.” <https://glaucus.crc.nd.edu/DUNEFluxes/>.
- [27] M. Masud, M. Bishai and P. Mehta, *Extricating New Physics Scenarios at DUNE with Higher Energy Beams*, *Sci. Rep.* **9** (2019) 352 [[1704.08650](#)].
- [28] J. Rout, S. Roy, M. Masud, M. Bishai and P. Mehta, *Impact of high energy beam tunes on the sensitivities to the standard unknowns at DUNE*, *Phys. Rev. D* **102** (2020) 116018 [[2009.05061](#)].
- [29] P.A.N. Machado, H. Nunokawa and R. Zukanovich Funchal, *Testing for Large Extra Dimensions with Neutrino Oscillations*, *Phys. Rev. D* **84** (2011) 013003 [[1101.0003](#)].
- [30] A. Di Iura, I. Girardi and D. Meloni, *Probing new physics scenarios in accelerator and reactor neutrino experiments*, *J. Phys. G* **42** (2015) 065003 [[1411.5330](#)].
- [31] J.M. Berryman, A. de Gouvêa, K.J. Kelly, O.L.G. Peres and Z. Tabrizi, *Large extra dimensions, the weak scale, and neutrino oscillations*, *Physical Review D* **94** (2016) 033006.

- [32] MINOS collaboration, *Constraints on Large Extra Dimensions from the MINOS Experiment*, *Phys. Rev. D* **94** (2016) 111101 [[1608.06964](#)].
- [33] MINOS, MINOS+ collaboration, *New results from MINOS and MINOS+*, *J. Phys. Conf. Ser.* **888** (2017) 012017.
- [34] C.A. Argüelles et al., *New opportunities at the next-generation neutrino experiments I: BSM neutrino physics and dark matter*, *Rept. Prog. Phys.* **83** (2020) 124201 [[1907.08311](#)].
- [35] DUNE collaboration, *Prospects for beyond the Standard Model physics searches at the Deep Underground Neutrino Experiment*, *Eur. Phys. J. C* **81** (2021) 322 [[2008.12769](#)].
- [36] D.V. Forero, C. Giunti, C.A. Ternes and O. Tyagi, *Large extra dimensions and neutrino experiments*, *Phys. Rev. D* **106** (2022) 035027 [[2207.02790](#)].
- [37] A.N. Khan, *Extra dimensions with light and heavy neutral leptons: an application to CE ν NS*, *JHEP* **01** (2023) 052 [[2208.09584](#)].
- [38] S. Roy, *Capability of the proposed long-baseline experiments to probe large extra dimension*, *Phys. Rev. D* **108** (2023) 055015 [[2305.16234](#)].
- [39] A. Giarnetti, S. Marciano and D. Meloni, *Exploring New Physics with Deep Underground Neutrino Experiment High-Energy Flux: The Case of Lorentz Invariance Violation, Large Extra Dimensions and Long-Range Forces*, *Universe* **10** (2024) 357 [[2407.17247](#)].
- [40] MINOS+ collaboration, *Search for sterile neutrinos in MINOS and MINOS+ using a two-detector fit*, *Phys. Rev. Lett.* **122** (2019) 091803 [[1710.06488](#)].
- [41] DAYA BAY collaboration, *Observation of electron-antineutrino disappearance at Daya Bay*, *Phys. Rev. Lett.* **108** (2012) 171803 [[1203.1669](#)].
- [42] KATRIN collaboration, *KATRIN: A Next generation tritium beta decay experiment with sub-eV sensitivity for the electron neutrino mass. Letter of intent*, [hep-ex/0109033](#).
- [43] DUNE collaboration, *Experiment Simulation Configurations Approximating DUNE TDR*, [2103.04797](#).
- [44] H. Davoudiasl, P. Langacker and M. Perelstein, *Constraints on large extra dimensions from neutrino oscillation experiments*, *Physical Review D* **65** (2002) 105015.
- [45] A. Esmaili, O.L.G. Peres and Z. Tabrizi, *Probing Large Extra Dimensions With IceCube*, *JCAP* **12** (2014) 002 [[1409.3502](#)].
- [46] P.A.N. Machado, H. Nunokawa, F.A.P. dos Santos and R.Z. Funchal, *Bulk Neutrinos as an Alternative Cause of the Gallium and Reactor Anti-neutrino Anomalies*, *Phys. Rev. D* **85** (2012) 073012 [[1107.2400](#)].
- [47] V.S. Basto-Gonzalez, A. Esmaili and O.L.G. Peres, *Kinematical Test of Large Extra Dimension in Beta Decay Experiments*, *Phys. Lett. B* **718** (2013) 1020 [[1205.6212](#)].

- [48] I. Girardi and D. Meloni, *Constraining new physics scenarios in neutrino oscillations from Daya Bay data*, *Phys. Rev. D* **90** (2014) 073011 [[1403.5507](#)].
- [49] W. Rodejohann and H. Zhang, *Signatures of Extra Dimensional Sterile Neutrinos*, *Phys. Lett. B* **737** (2014) 81 [[1407.2739](#)].
- [50] M. Carena, Y.-Y. Li, C.S. Machado, P.A.N. Machado and C.E.M. Wagner, *Neutrinos in Large Extra Dimensions and Short-Baseline ν_e Appearance*, *Phys. Rev. D* **96** (2017) 095014 [[1708.09548](#)].
- [51] G.V. Stenico, D.V. Forero and O.L.G. Peres, *A Short Travel for Neutrinos in Large Extra Dimensions*, *JHEP* **11** (2018) 155 [[1808.05450](#)].
- [52] V.S. Bastro-Gonzalez, D.V. Forero, C. Giunti, A.A. Quiroga and C.A. Ternes, *Short-baseline oscillation scenarios at JUNO and TAO*, *Phys. Rev. D* **105** (2022) 075023 [[2112.00379](#)].
- [53] R.N. Mohapatra and A. Perez-Lorenzana, *Three flavor neutrino oscillations in models with large extra dimensions*, *Nucl. Phys. B* **593** (2001) 451 [[hep-ph/0006278](#)].
- [54] P. Huber, M. Lindner and W. Winter, *Simulation of long-baseline neutrino oscillation experiments with GLoBES (General Long Baseline Experiment Simulator)*, *Comput. Phys. Commun.* **167** (2005) 195 [[hep-ph/0407333](#)].
- [55] P. Huber, J. Kopp, M. Lindner, M. Rolinec and W. Winter, *New features in the simulation of neutrino oscillation experiments with GLoBES 3.0: General Long Baseline Experiment Simulator*, *Comput. Phys. Commun.* **177** (2007) 432 [[hep-ph/0701187](#)].
- [56] GEANT4 collaboration, *GEANT4: A Simulation toolkit*, *Nucl. Instrum. Meth.* **A506** (2003) 250.
- [57] J. Allison et al., *Geant4 developments and applications*, *IEEE Trans. Nucl. Sci.* **53** (2006) 270.
- [58] A. De Gouvêa, K.J. Kelly, G. Stenico and P. Pasquini, *Physics with Beam Tau-Neutrino Appearance at DUNE*, *Phys. Rev. D* **100** (2019) 016004 [[1904.07265](#)].
- [59] A. Ghoshal, A. Giarnetti and D. Meloni, *On the role of the ν_τ appearance in DUNE in constraining standard neutrino physics and beyond*, *JHEP* **12** (2019) 126 [[1906.06212](#)].
- [60] P. Machado, H. Schulz and J. Turner, *Tau neutrinos at DUNE: New strategies, new opportunities*, *Phys. Rev. D* **102** (2020) 053010 [[2007.00015](#)].
- [61] DUNE collaboration, *Experiment Simulation Configurations Used in DUNE CDR*, [1606.09550](#).
- [62] P. Huber, M. Lindner and W. Winter, *Superbeams versus neutrino factories*, *Nucl. Phys.* **B645** (2002) 3 [[hep-ph/0204352](#)].
- [63] G.L. Fogli, E. Lisi, A. Marrone, D. Montanino and A. Palazzo, *Getting the most from the statistical analysis of solar neutrino oscillations*, *Phys. Rev.* **D66** (2002) 053010 [[hep-ph/0206162](#)].

- [64] M. Gonzalez-Garcia and M. Maltoni, *Atmospheric neutrino oscillations and new physics*, *Phys.Rev.* **D70** (2004) 033010 [[hep-ph/0404085](#)].
- [65] R. Gandhi, P. Ghoshal, S. Goswami, P. Mehta, S.U. Sankar and S. Shalgar, *Mass Hierarchy Determination via future Atmospheric Neutrino Detectors*, *Phys. Rev.* **D76** (2007) 073012 [[0707.1723](#)].
- [66] X. Qian, A. Tan, W. Wang, J.J. Ling, R.D. McKeown and C. Zhang, *Statistical Evaluation of Experimental Determinations of Neutrino Mass Hierarchy*, *Phys. Rev.* **D86** (2012) 113011 [[1210.3651](#)].
- [67] GALLEX collaboration, *Final results of the Cr-51 neutrino source experiments in GALLEX*, *Phys. Lett. B* **420** (1998) 114.
- [68] SAGE collaboration, *Measurement of the response of the Russian-American gallium experiment to neutrinos from a Cr-51 source*, *Phys. Rev. C* **59** (1999) 2246 [[hep-ph/9803418](#)].
- [69] V.V. Barinov et al., *Results from the Baksan Experiment on Sterile Transitions (BEST)*, *Phys. Rev. Lett.* **128** (2022) 232501 [[2109.11482](#)].
- [70] J.C. Long, H.W. Chan and J.C. Price, *Experimental status of gravitational strength forces in the subcentimeter regime*, *Nucl. Phys. B* **539** (1999) 23 [[hep-ph/9805217](#)].
- [71] D.E. Krause and E. Fischbach, *Searching for extra dimensions and new string inspired forces in the Casimir regime*, *Lect. Notes Phys.* **562** (2001) 292 [[hep-ph/9912276](#)].
- [72] E. Fischbach, D.E. Krause, V.M. Mostepanenko and M. Novello, *New constraints on ultrashort ranged Yukawa interactions from atomic force microscopy*, *Phys. Rev. D* **64** (2001) 075010 [[hep-ph/0106331](#)].
- [73] EOT-WASH GROUP collaboration, *Sub-millimeter tests of the gravitational inverse square law*, in *2nd Meeting on CPT and Lorentz Symmetry*, pp. 9–15, 2002, DOI [[hep-ex/0202008](#)].
- [74] R.S. Decca, E. Fischbach, G.L. Klimchitskaya, D.E. Krause, D.L. Lopez and V.M. Mostepanenko, *Improved tests of extra dimensional physics and thermal quantum field theory from new Casimir force measurements*, *Phys. Rev. D* **68** (2003) 116003 [[hep-ph/0310157](#)].
- [75] T.G. Rizzo, *More and more indirect signals for extra dimensions at more and more colliders*, *Phys. Rev. D* **59** (1999) 115010 [[hep-ph/9901209](#)].
- [76] J.L. Hewett, *Indirect collider signals for extra dimensions*, *Phys. Rev. Lett.* **82** (1999) 4765 [[hep-ph/9811356](#)].
- [77] D0 collaboration, *Search for large extra dimensions in dielectron and diphoton production*, *Phys. Rev. Lett.* **86** (2001) 1156 [[hep-ex/0008065](#)].
- [78] DELPHI collaboration, *Measurement and interpretation of fermion-pair production at LEP energies of 183-GeV and 189-GeV*, *Phys. Lett. B* **485** (2000) 45 [[hep-ex/0103025](#)].

- [79] DELPHI collaboration, *Search for one large extra dimension with the DELPHI detector at LEP*, *Eur. Phys. J. C* **60** (2009) 17 [[0901.4486](#)].
- [80] S. Cullen and M. Perelstein, *SN1987A constraints on large compact dimensions*, *Phys. Rev. Lett.* **83** (1999) 268 [[hep-ph/9903422](#)].
- [81] V.D. Barger, T. Han, C. Kao and R.-J. Zhang, *Astrophysical constraints on large extra dimensions*, *Phys. Lett. B* **461** (1999) 34 [[hep-ph/9905474](#)].
- [82] C. Hanhart, D.R. Phillips, S. Reddy and M.J. Savage, *Extra dimensions, SN1987a, and nucleon-nucleon scattering data*, *Nucl. Phys. B* **595** (2001) 335 [[nucl-th/0007016](#)].
- [83] S. Hannestad and G. Raffelt, *New supernova limit on large extra dimensions*, *Phys. Rev. Lett.* **87** (2001) 051301 [[hep-ph/0103201](#)].
- [84] S. Hannestad and G.G. Raffelt, *Supernova and neutron star limits on large extra dimensions reexamined*, *Phys. Rev. D* **67** (2003) 125008 [[hep-ph/0304029](#)].
- [85] R.N. Mohapatra, S. Nussinov and A. Perez-Lorenzana, *Large extra dimensions and decaying KK recurrences*, *Phys. Rev. D* **68** (2003) 116001 [[hep-ph/0308051](#)].
- [86] J.L. Feng, A. Rajaraman and F. Takayama, *Graviton cosmology in universal extra dimensions*, *Phys. Rev. D* **68** (2003) 085018 [[hep-ph/0307375](#)].
- [87] G. Cacciapaglia, M. Cirelli and A. Romanino, *Signatures of supernova neutrino oscillations into extra dimensions*, *Phys. Rev. D* **68** (2003) 033013 [[hep-ph/0302246](#)].
- [88] L.J. Hall and D. Tucker-Smith, *Cosmological constraints on theories with large extra dimensions*, *Phys. Rev. D* **60** (1999) 085008 [[hep-ph/9904267](#)].
- [89] S. Hannestad, *Strong constraint on large extra dimensions from cosmology*, *Phys. Rev. D* **64** (2001) 023515 [[hep-ph/0102290](#)].
- [90] M. Fairbairn, *Cosmological constraints on large extra dimensions*, *Phys. Lett. B* **508** (2001) 335 [[hep-ph/0101131](#)].
- [91] M. Fairbairn and L.M. Griffiths, *Large extra dimensions, the galaxy power spectrum and the end of inflation*, *JHEP* **02** (2002) 024 [[hep-ph/0111435](#)].
- [92] H.S. Goh and R.N. Mohapatra, *Big bang nucleosynthesis constraints on bulk neutrinos*, *Phys. Rev. D* **65** (2002) 085018 [[hep-ph/0110161](#)].
- [93] PARTICLE DATA GROUP collaboration, *Review of Particle Physics*, *PTEP* **2022** (2022) 083C01.
- [94] C. Sanderson and R. Curtin, *Armadillo: a template-based c++ library for linear algebra*, *Journal of Open Source Software* **1** (2016) 26.
- [95] C. Sanderson and R. Curtin, *Practical sparse matrices in c++ with hybrid storage and template-based expression optimisation*, *Mathematical and Computational Applications* **24** (2019) .